DEFINING INPUT TUMOR CELL PHENOTYPES FOR MICROPHYSIOLOGICAL

MODELS OF CANCER

A THESIS

SUBMITTED ON THE 5th DAY OF MAY, 2023

TO THE DEPARTMENT OF BIOMEDICAL ENGINEERING
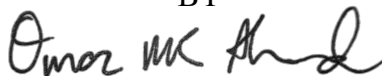
OF

TULANE UNIVERSITY

FOR THE DEGREE OF

MASTER OF SCIENCE

IN BIOMEDICAL ENGINEERING

BY

_____

OMAR MUSTAFA KAMAL AHMAD

APPROVED:

_____

MARK J. MONDRINOS, PhD

Director of Thesis

_____

J. QUINCY BROWN, PhD

Second Reader

_____

MATTHEW E. BUROW, PhD

Third Reader

1

ABSTRACT

Lung cancer is the leading cause of cancer-related death worldwide and breast cancer is the most diagnosed type of cancer. This thesis describes efforts to develop microphysiological models of drug-resistant non-small cell lung cancer (NSCLC) and triple negative breast cancer (TNBC). Microphysiological models of cancer should serve as assays capable of quantifying the differences in key properties of the tumor microenvironment that influence progression and metastasis in different individuals and during the course treatment-induced tumor evolution. We demonstrate that cisplatin resistance increases the expression of genes associated with mesenchymal transition, inflammatory cytokine production, and angiogenesis relative to parent NSCLC cells in 2D and 3D cultures of NSCLC cells. We then quantified the functional significance of these input tumor cell phenotypes using a microphysiological model of cancer-induced angiogenesis. We found that cisplatin resistant phenotypes drive a significant increase in sprouting across multiple metrics, which could help explain the increased aggressivity and speed of progression in patients with recurrent NSCLC after cisplatin therapy. Using similar biochemical assays and microphysiological modeling approaches, we measured reduced expression of proinflammatory genes in TNBC cells with the ERK5 gene knocked out. Previous studies demonstrated reduced angiogenesis in a tumor xenograft model using the same ERK5-/- TNBC cells. We measured significantly reduced mRNA for the cytokines IL-1B and IL-6, both of which are strongly correlated with cancer angiogenesis. We then tested the hypothesis that ERK5 knockout would significantly decrease cancer-induced sprouting angiogenesis. Future work will focus on modeling more complex drug resistance scenarios in NSCLC and developing

2

microphysiological assays to define the impact of drug resistant tumor cell phenotypes on cancer angiogenesis, metastasis, and cachexia. In addition, we will continue to explore ERK5 as a target in TNBC, with a shift to focusing on quantifying individual responses to pharmacological inhibition of ERK5 in patient-derived models.

3

DEFINING INPUT TUMOR CELL PHENOTYPES FOR MICROPHYSIOLOGICAL

MODELS OF CANCER

A THESIS

SUBMITTED ON THE 5th DAY OF MAY, 2023

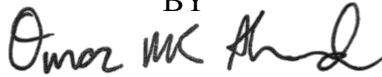TO THE DEPARTMENT OF BIOMEDICAL ENGINEERING

OF

TULANE UNIVERSITY

FOR THE DEGREE OF

MASTER OF SCIENCE

IN BIOMEDICAL ENGINEERING

BY

_____

OMAR MUSTAFA KAMAL AHMAD

APPROVED:

_____

MARK J. MONDRINOS, PhD

Director of Thesis

_____

J. QUINCY BROWN, PhD

Second Reader

_____

MATTHEW E. BUROW, PhD

Third Reader

1

ACKNOWLEDGEMENTS

Dedicated to my parents, Dr. Safeer Ahmad and Azra Ahmad, and sister, Bushra Ahmad

for their undoubted love and support the past 23 years,

my principal investigator and mentor, Dr. Mark J. Mondrinos,

for inspiring me to pursue tissue engineering research,

my lab mate and friend, Elisabet A. Olsen,

for always being by my side,

all the people I've met at Tulane

for helping me find my life's purpose.

and Susan Spaid DelCorral,

my best friend's late mom,

for inspiring me to pursue cancer research.

4

TABLE OF CONTENTS

6

LIST OF TABLES

7

LIST OF FIGURES

8

CHAPTER 1: INTRODUCTION

Cancer represents one of the medicine's tallest battles, accounting for nearly 19.3 million new cases and 10 million deaths, globally in 2020.[1] Of all cancer types, breast and lung cancer are the two most commonly diagnosed cancers with an estimated 2.3 million new cases of breast cancer and 2.2 million new cases of lung cancer.[1] Lung cancer encompasses two main types – non-small cell lung cancer (NSCLC) and small cell lung cancer (SCLC) – with NSCLC being further subdivided into lung adenocarcinoma, squamous cell carcinoma, and large cell carcinoma.[2] Of all the NSCLC subtypes, lung adenocarcinoma is the most prevalent, accounting for approximately 40% of all total lung cancer cases[3]. Breast cancer is classified upon hormone receptor status and molecular characteristics. While there are numerous breast cancer subtypes, triple negative breast cancer (TNBC) is the most aggressive subtype with poorer clinical outcomes, accounting for nearly 15-20% of all breast cancer cases[4]. What makes TNBC particularly challenging to treat is that it lacks the expression of estrogen receptor (ER), progesterone receptor (PR), and human epidermal growth factor receptor 2 (HER2).[5] These figures highlight the urgency needed to develop better treatment options, which starts with engineering more physiologically relevant *in vitro* models that aid in drug development. Organs-on-a-chip (OoaCs) are widely known for being more physiologically relevant and high-throughput than traditional tissue culture systems and animal models.[6,7,8,9] In order for OoaCs to accurately recapitulate human physiology, many parameters (i.e., cells/tissues, ECM composition, fluidic conditions, and microenvironment interfaces) must be optimized[7,10].

9

1.1: NON-SMALL CELL LUNG CANCER

The primary cause of lung cancer is smoking, particularly in countries where smoking is a common habit[11]. While global efforts to curb tobacco help, other factors such as pollution, occupational carcinogens, second-hand smoking and genetic predisposition can also contribute to lung cancer.[1,11] The 5-year overall survival rate for lung cancer varies depending upon tumor stage from 83% for stage IA to 36% for stage IIIA.[11] Complete tumor resection is the most effective treatment option for stages I-II while later stage III-IV typically employ platinum-based doublet therapy.

1.1A: CISPLATIN RESISTANCE

Drug resistance in represents a major hurdle in the treatment of NSCLC, frequently leading to relapse and poor clinical outcomes[12,13]. Cisplatin (cis-diamminedichloroplatinum (II)) is one of the most popular platinum-based chemotherapies used for NSCLC[14]. Cisplatin treatment after five years leads to a 6.9% decrease in lung cancer associated deaths, compared to untreated control[15].

Cisplatin's defined effects are not well understood but it's known to cause DNA damage and induce apoptosis, thereby inhibiting growth and proliferation of cancer cells[16]. Initially, administration of cisplatin often leads to therapeutic success, however, many patients inevitably adopt resistance to cisplatin[17]. Resistance arises when cisplatin-treated cancer cells can proliferate and survive[16]. Cisplatin resistance is either intrinsic or rapidly adopted through a variety of mechanisms by cancer cells. Intrinsic cisplatin resistance is not well understood but can result from acute extracellular folate (vitamin B) deprivation[18]. Rapidly adopted cisplatin

10

resistance mechanisms can be categorized based on cellular target: pre-target, on-target, post-target, and off-target. Targeting only one mechanism has poor efficacy in overcoming cisplatin resistance since it usually implicates a combination of mechanisms. However, understanding these mechanisms can provide a systematic approach towards overcoming cisplatin resistance[17].
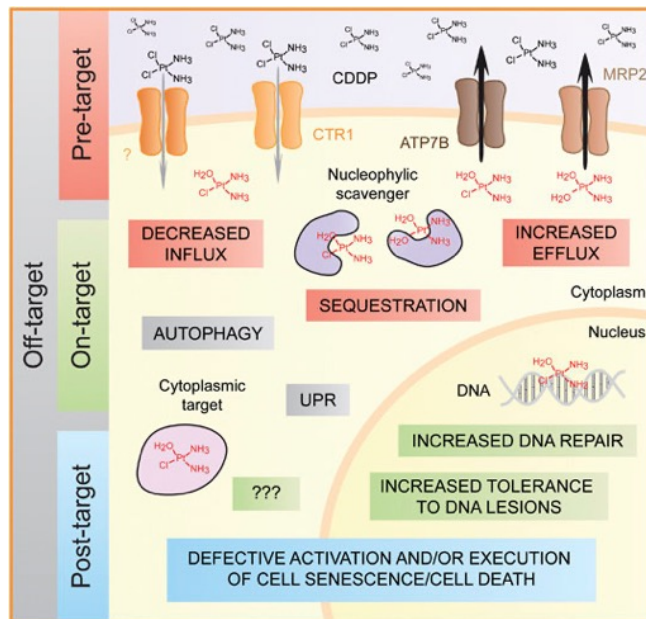
Figure 1: Molecular mechanisms of cisplatin resistance. Mechanisms can be categorized by cellular target: pre-target, on-target, post-target, and off-target.[13]

1.1B: EPITHELIAL-TO-MESENCHYMAL TRANSITION (EMT)

Nearly 90% of all cancers originate from epithelial tissue, including NSCLC[19]. Epithelial cells are columnar shaped cells that line the basement membrane of several organs creating an apical-basal polarity[20]. Neighboring epithelial cells along the basement membrane have a high degree of cell-to-cell adhesion with tight junctions and desmosomes[20]. Epithelial cells possess a high differentiation potential; however, they can detach from the basement membrane and migrate to

11

surrounding organs[20]. This dissemination of cancerous epithelial cells to distal organs is another part of tumor aggression that is a prospective therapeutic target. When malignant epithelial migrate, they often undergo a process called epithelial-to-mesenchymal transition (EMT) which leads to the loss of their cell-to-cell junctions and apical-basal polarity, adoption of stem cell-like features, and transition towards a mesenchymal cell phenotype[21].

Mesenchymal cells adopt a spindle-like shape with a front-to-back polarity[20]. They have a high migratory potential and are not highly differentiable like epithelial cells[20]. After an epithelial cell transitions into a mesenchymal phenotype, they can invade neighboring tissues where they can undergo the reverse of EMT called the mesenchymal-to-epithelial transition (MET) that allows them to re-initiate tumor metastasis[22].
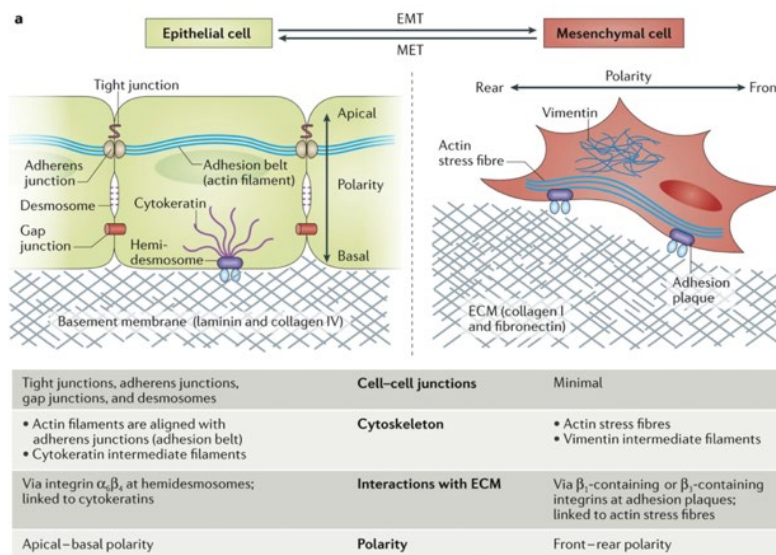
Figure 2: An overview of EMT-associated changes in cell physiology.[23]

EMT-contributed tumor colonization does not require a complete conversion to mesenchymal state, though[21]. A partial mesenchymal state is sufficient to initiate tumor metastasis[21]. There are

12

several subtypes of tumors that are associated with partial EMT stages[24]. These intermediate

stages are consistent with the heterogeneous nature of tumor[24]. Cells that partially undergo EMT

can revert to epithelial type cells via MET[24]. Once cells are fully mesenchymal it is potentially

irreversible but this is largely dependent on cell type[24]. Moreover, complete mesenchymal

transition is rarely observed in cancer[19].

EMT is a major contributor to drug resistance. Anti-tumor drugs are unable to target cells once

they've become a cancer stem cell (CSC) via the EMT[23]. In addition to evading drug

therapeutics, CSCs have the capacity to self-renew which leads to tumor relapse[23]. Several

stimuli and signaling pathways contribute to EMT induction. For example, TGFB-SMAD

signaling can be triggered by specific signals from stromal cells in the tumor microenvironment

due to various inflammatory and hypoxic insults[20].
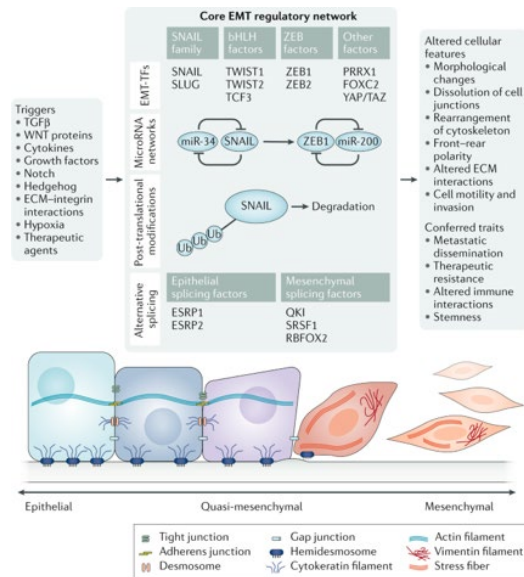
Figure 3: Overview of regulatory factors mediating EMT.[25]

13

1.1C: ANGIOGENESIS

Angiogenesis, the process by which new blood vessels are formed from pre-existing vasculature and is well controlled in normal physiological processes such as wound healing[26]. However, it plays a critical role in the progression of tumor growth by supplying oxygen and nutrients to the tumor and its microenvironment. Angiogenesis both facilitates tumor growth and drives metastasis as newly formed vasculature provides the primary tumor routes for cancer cell dissemination to distal sites[27]. The initiation of angiogenesis is said to be dependent upon an angiogenic "switch," which leads to a complex series of events, starting with the release of proangiogenic factors and endothelial cell activation. Modulation of this angiogenic switch is balanced by intrinsic pro-angiogenic and anti-angiogenic factors within the tumor microenvironment[28].

Quintessential growth factors such as vascular endothelial growth factor (VEGF) and fibroblast growth factor (FGF) not only contribute to angiogenesis, but also drive endothelial cell proliferation, migration, and tube formation[29].
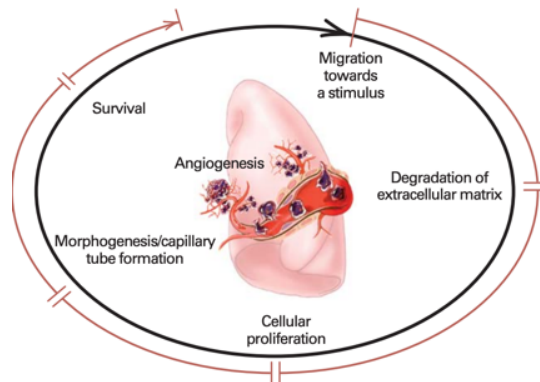
Figure 4: The multistep process of angiogenesis.[28]

14

Since Folkman's discovery in 1971, angiogenesis has emerged as a promising target for cancer treatment as targeting angiogenic pathways can inhibit tumor growth, suppress metastatic potential, and normalize tumor vasculature, thereby enhancing delivery and efficacy of other drug treatments[26]. For example, bevacizumab, a monoclonal antibody targeting VEGF, has demonstrated efficacy in combination with chemotherapy for the treatment of NSCLC[30]. Despite initial efficacy of anti-angiogenic treatments, resistance and the potential for tumor invasiveness remain significant challenges[31]. Further investigation into the complex interplay between tumor cells, the microenvironment, and angiogenic signaling is necessary in order to optimize anti-angiogenic agents and improve outcomes for lung cancer patients.

1.1D: CHALLENGES WITH RECAPITULATING DRUG RESISTANCE IN VITRO

Several limitations are associated with the development of cisplatin-resistant A549s and these ultimately depend upon the investigator's interest. Maintaining relevance to the clinic might seem like an obvious goal but this often necessitates lower drug concentrations that yield smaller, nearly imperceptible molecular changes. These lower drug concentrations are typically administered in pulsed treatments that are shorter in culture time as compared to high-level models and then reverted to drug-free media. Increasing drug concentrations reduces clinical relevancy but it magnifies various molecular pathways involved in toxicity and resistance. Even though clinically relevant models only maintain a nearly 2-5x fold increase in IC50 from parental cell line, resistance is often unstable and eventually lost after repeated repassaging. This presents a major concern for engineering high-throughput models that enable the screening of anti-metastatic therapies.

15

High-level models lose their relevancy to the clinic due to their increased drug concentrations, typically resulting in a 20x fold increase in IC50 from parental cell line. Administering such a high dose of chemotherapy to a parental line in such a short period of time can lead to all cells dying. Therefore, doses are increased overtime in culture to reach such a stark increase in IC50. This has its limitations, though, as culturing these models can take up to 18 months which restricts high-throughput capacity. Moreover, maintaining these cells in culture with drug leads to highly stable resistance.

Short-Term Protocols	Long-Term Protocols
Pulsed drug treatment	Escalating drug treatment
More relevant to the clinic	Less relevant to the clinic
Unstable, low-level resistance	Highly stable resistance
Small, imperceptible molecular changes	Large, discernable molecular changes

Table 1: Comparison of two different models for culturing drug resistance, adapted from McDermott, M., et al. (2014).[32]

1.2: TRIPLE-NEGATIVE BREAST CANCER

The exact cause of TNBC is not as well characterized as with lung cancer; however, genetic predisposition, hormonal factors, and environmental exposures have been proposed to contribute to TNBC development[33]. TNBC disproportionately affects younger women, African American women, and those with BRCA1 mutations[5,34].

The lack of ER, PR, and HER2 receptor expression limits treatment options for TNBC, and chemotherapies such as cisplatin, paclitaxel, and doxorubicin, among others, remain the standard treatment for TNBC; however, this often results in poorer clinical outcomes with nearly all women with metastatic TNBC ultimately die[35,36].

1.2A: EPITHELIAL-TO-MESENCHYMAL TRANSITION

TNBC has been associated with increased EMT markers and enhanced migratory and invasive properties as compared to other breast cancer subtypes[37,38]. EMT helps us understand, in part, TNBC's aggressive behavior, metastasis, and resistance to therapy[37,38]. Multiple pathways have been implicated in EMT induction in TNBC including transforming growth factor-beta (TGFB), Wnt/B-catenin, and Notch[39].

Given the significant role EMT plays in TNBC progression and metastasis, targeting key EMT regulators and signaling pathways presents a promising therapeutic strategy. Moreover, several drugs have been identified that can inhibit EMT that aid in the inhibition of TNBC progression and metastasis[38].

1.2B: ERK5 ROLE IN TNBC

17

Extracellular signal-regulated kinase 5 (ERK5), also known as mitogen-activated protein kinase 7 (MAPK7), is a member of the mitogen-activated protein kinase family and plays an essential role in regulating cellular proliferation, survival, differentiation, and motility[40]. ERK5 signaling is activated in response to various stimuli, such as growth factors and cytokines[41] Following initial activation of the ERK5 pathway with said stimuli, a cascade of intracellular kinases, including MAPK kinase 3 (MEKK3) and MAPK kinase 5 (MEK5) activate ERK5 via phosphorylation[41]. Activated ERK5 can translocate to the nucleus wherein it phosphorylates and regulates the activity of various transcription factors implicated in cellular proliferation, survival, and migration such as c-Myc, c-Fos, and MEF2[42].

Recent studies have reported that ERK5 is overexpressed in a subset of TNBC types and its expression levels have been correlated with poorer clinical outcomes, including shorter overall survival, higher rates of distant metastasis[43]. Overexpression of ERK5 has also been associated with increased proliferation, migration, and invasion of TNBC cells in vitro, suggesting a role for ERK5 in the angiogenesis axis for TNBC[40,43]. Moreover, ERK5 has recently been implicated in the regulation of the ECM in TNBC tumor formation and deletion of ERK5 expression using CRISPR/Cas9 in TNBC has resulted in suppression of TNBC cell migration[40].

Taken together, ERK5 signaling in the progression of TNBC underscores the need for further investigation for ERK5 inhibitors as a potential therapeutic target against TNBC.

18

1.3: ROLE OF MICROPHYSIOLOGICAL SYSTEMS AND ORGAN-ON-A-CHIP MODELS IN ONCOLOGIC RESEARCH AND PERSONALIZED MEDICINE MICROPHYSIOLOGICAL SYSTEMS AND BIOLOGICAL MICRO-ELECTRO-MECHANICAL SYSTEMS

Microphysiological systems (MPS) are advanced *in vitro* models that aims to recapitulate the structural, functional, and physiological characteristics of human organs and tissues on a microfluidic scale[44]. These systems often integrate multiple cell types and cellular components within a 3D microenvironment and incorporate dynamic factors such as fluid flow, mechanical forces, and chemical gradients of signaling molecules to more accurately mimic *in vivo* conditions. Biological Micro-Electro-Mechanical Systems (BioMEMS) refer to a subset of MEMS technology that involve microscale electronic and mechanical systems to interface with biological systems to perform sensing, actuation, or both, for applications in diagnostics and drug delivery[45].

Early efforts in this field focused on leveraging microfabrication techniques from the microelectronics industry to create microscale devices capable of manipulating and characterizing biological samples *in vitro*[46]. MPS and BioMEMS have shown significant potential for providing more physiologically relevant *in vitro* platforms that closely mimic *in vivo* pathologies[44]. By recapitulating key cellular and tissue-level features, these systems enable a more accurate assessment complex pathophysiology that were otherwise difficult to assess *in vitro* without utilization of animal models[47]. Consequently, the insights gained from these models

19

can pave the development of novel cancer therapeutics and inform the selection of patient-specific treatments in efforts to improve clinical outcomes.

1.3A: ORGANS-ON-A-CHIP

Organs-on-a-chip (OoaCs) are a subset of MPS that focus on recapitulating the microarchitecture and function of specific organs[44]. These systems conventionally employ microfluidics, biomaterials, and cellular components to create a three-dimensional, dynamic, physiologically relevant environment that closely aligns with *in vivo* conditions[48,49]. Various OoaCs have been developed for various organs, including lung, liver, and heart, and have even been combined to model multi-organ interactions with significant physiological relevance[48,50–52].
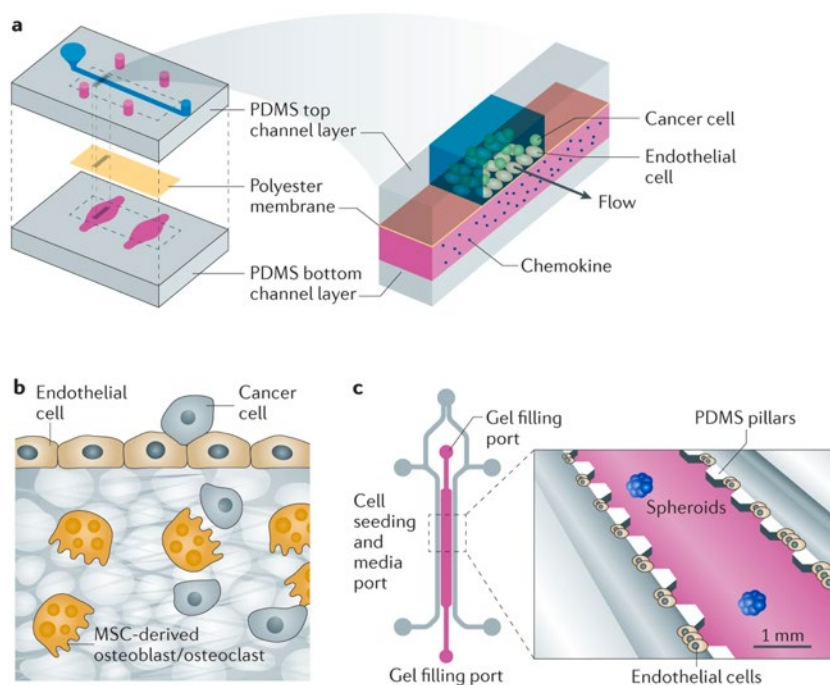
Figure 5: Organ-on-a-chip models for cancer research[7].

OoaCs have significantly accelerated drug discovery and development for being higher-throughput than animal models[44,53]. This is largely in part due to their miniaturized and scalable nature, which facilitates the parallel assessment of multiple drug candidates, concentrations, and combinations[54]. Furthermore, microfluidics in OoaCs enable precise control over the cellular microenvironment which allow for the standardization and real-time monitoring of cellular responses to drug exposure and the assessment of pharmacokinetics and pharmacodynamics[55,56]. Not only do OoaCs provide great promise for streamlining and standardizing drug discovery pipelines, but OoaCs also reduce the cost and time associated with traditional *in vitro* and animal models[53,54].

1.3B: 3D PRINTING

Much of the scalability and reproducibility of OoaCs is attributed to 3D printing techniques which facilitate the production of OoaCs with consistent, standardized designs[57,58]. Specifically, 3D printing techniques, such as stereolithography, inkjet printing, and extrusion-based printing, enable the precise fabrication of OoaCs with intricate, multi-layered microstructures that closely mimic native tissue architecture and cellular interactions[59,60].

3D bioprinting can be employed to deposit cells, biomaterials, and ECM components layer-by-layer, constructing OoaCs with spatially controlled organization of multiple cell types and ECM compositions, thus depicting the heterogeneity and structural complexity of human tissue[60,61]. This capability enhances the biological relevance of OoaCs while also allowing for the creation of patient-specific models, providing a more accurate platform for drug testing and development.

21

1.3C: SOFT-LITHOGRAPHY

Soft-lithography techniques have also played a critical role in the fabrication of OoaCs. Soft

lithography is a family of techniques that includes replica molding, microcontact printing, and

microfluidic patterning while leveraging elastomeric materials such as polydimethylsiloxane

(PDMS) to create intricate, microscale structures with high resolution and fidelity[62,63]. Replica

molding is a technique that involves casting a liquid prepolymer onto a master mold to create a

replica of the mold's features; microcontact printing involves transferring patterns of self-

assembled monolayers or biomolecules from a stamp to a substrate[62,63].

In the context of OoaCs, soft lithography can be leveraged to design and fabricate microfluidic

channels and compartments that simulate the complex vascular and interstitial networks found in

native physiological tissues. These microscale features enable precise control over the nutrient

delivery, excretion, and intercellular communication of the cellular microenvironment, thereby

promoting the generation of physiologically relevant OoaCs[44,64].

1.3D: PERSONALIZED MEDICINE

The intersection of MPS, OoaCs, 3D printing, and soft-lithography techniques provide a

promising avenue for the development of patient-specific cancer models that can inform

personalized medicine strategies[7,44]. For instance, patient-derived organoids and tumor-on-a-chip

models have been utilized to assess individual drug responses and predict optimal therapeutic

strategies in various types of cancer, including colorectal, breast, and lung cancer[65–67].

Additionally, OoaCs have been employed to investigate the role of stromal interactions with

22

tumors and how they may influence drug resistance, thereby providing insights that may aid in the development of personalized combination therapies[68].

Moreover, the integration of OoaCs with single-cell sequencing, among other advanced analytical technologies, can provide critical insights on the molecular basis of patient tumor heterogeneity. Furthermore, the deployment of OoaCs in clinics and hospitals in a point-of-care fashion can further elucidate patient therapeutic response to specified drugs, thereby enabling real-time, data-driven clinical decision-making that allows providers the essential tools to optimize treatment strategies and minimize trial-and-error approaches[69,70].

1.4: OBJECTIVES

When generating cisplatin-resistant lung adenocarcinoma tissues, we aim to focus on capturing characteristics in line with more mesenchymal and angiogenic cell populations, as both EMT and angiogenesis are associated with more aggressive forms of lung adenocarcinoma. This starts by validating an optimal treatment protocol that yields resistant cell populations in a relatively short period of time, when compared to longer month or yearlong protocols. It's our aim that this shorter time will make recapitulating drug resistance *in vitro* higher throughput for organ-on-a-chip applications. Furthermore, we aim to characterize parameters within said optimal treatment protocol that can be used for other researchers quality control when rapidly producing cisplatin-resistant cells from parental A549s. We then aim to leverage our lab's previously described double lane membrane-free organ-on-a-chip device to investigate differences in angiogenic sprouting between cisplatin-resistant and parental A549s. Following this, we hope to translate approaches from cisplatin-resistance in lung adenocarcinoma to validate ongoing work from our

23

collaborators finding that ERK5-/- tissues exhibit reduced vessel formation, relative to parental

TNBC tumors, by finding less angiogenic sprouting in our double lane membrane-free organ-on-

a-chip.

24

CHAPTER 2: METHODS

2.1: 2D CELL CULTURE

Both parental A549 and MDA-MB-231 cells were obtained from American Type Culture

Collection (CRM-CCL-185; CRM-HTB-26). A549 cells were cultured in F-12K culture medium

(10% fetal bovine serum and 1% antibiotic-antimycotic) whereas MDA-MB-231 cells were

cultured in DMEM media (10% fetal boxine serum, 1% antibiotic-antimycotic, 1% essential

amino-acids, 1% non-essential amino acids, and 5uL insulin). Passage-matched MDA-MB-231

cells were CRISPR/Cas9 knocked out for ERK5 by the Burow Lab at Tulane University. Human

Lung Fibroblasts (HLF) were obtained from ATCC and were cultured in ATCC Fibroblast

Growth Medium with 2% fetal bovine serum and 1% antibiotic-antimycotic. Human Umbilical

Vein Endothelial Cells (HUVEC) were also obtained from ATCC and cultured in ATCC

Vascular Endothelial Growth Medium, supplemented with Vascular Growth Kit with VEGF and

1% antibiotic-antimycotic. All cell culture lines were incubated at 5% CO_2 and 37ºC.

2.2: ACUTE 96 HOUR CISPLATIN TREATMENT IN A549 CELLS

Cisplatin (Selleckchem S1166) was dissolved in sterile deionized water and frozen at -80ºC in

amber tubes. At time of cisplatin administration, aliquots were briefly thawed in water bath at

37ºC. Once parent A549s were ~70% confluent, T25 flask is administered 25uM cisplatin

directly from thawed stock into F-12K medium

2.3: 3D SPHEROID CULTURE

A549 spheroids were seeded at 1,000 cells/well in a 96 well round bottom plate (ThermoFisher

262162) and cultured for 4 days in 100uL F12K media per well. MDA-MB-231 spheroids were

25

also seeded at 1,000 cells/well in a 96 well round bottom plate but after 24 hours, received

additional 100uL DMEM media with 3ug/mL collagen type I (Corning 354236) and were

centrifuged at 100g for 3 minutes after 24 hours from seeding to promote spheroid formation.

Elplasia spheroids were seeded at 3,000 cells/well in a 96 well Elplasia microcavity plate

(Corning 4442).

2.4: REAL-TIME QUANTITATIVE POLYMERASE CHAIN REACTION (RT-qPCR)

2.4A: RNA Isolation

A549 and MDA-MB-231 RNA was stored at 4ºC for no more than 1 month in RNALater

solution (Invitrogen AM7020). RNA Isolation of A549 and MDA-MB-231 tissues were

performed in accordance with Qiagen's RNeasy kit (ID: 74104). After RNA isolation, nanodrop

spectrophotometer was used to measure RNA concentration and sample purity (260/280 and

260/230 ratios). Samples with <95ng/uL concentration, and purity 260/280 and 260/230 outside

2.0 ± 0.3 were excluded. RNA samples were stored in -80ºC until cDNA synthesis.

2.4B: cDNA Synthesis

cDNA synthesis using Quantabio qScript cDNA SuperMix (95048-100) was performed in a

thermocycler under the following conditions: 25.0ºC for 5 min; 42.0ºC for 30 min; 85ºC for 5

min; 4ºC hold. Following cDNA synthesis reaction, the 20uL cDNA sample was diluted 1:10

with nuclease-free water and stored at -20ºC until RT-qPCR reaction.

2.5C: Primer Design

Gene-specific primers were designed using the Primer-BLAST tool from the National Center for

Biotechnology Information (NCBI) with a maximum PCR product size of 200 and $T_m = 60ºC \pm$

26

3ºC. Custom DNA Oligo primers were ordered from Integrated DNA Technologies with the following specifications: 25 nmole DNA Oligo; Standard Desalting Purification; LabReady (Normalized to 100uM in IDTE pH 8.0). Primer sequences are provided in Appendix A. Working primer was prepared by diluting 1:20 of both the forward and reverse DNA Oligo in nuclease-free water and stored at 4ºC.

2.5D: RT-qPCR Reaction Setup

Reactions were carried out using the Power SYBR Green Master Mix (Applied Biosystems, 4368577) in a 96-well format. Each 20uL reaction consisted of 10uL Power SYBR Green Master Mix, 1uL Working Primer, 6uL nuclease-free water, and 3uL cDNA. All reactions were carried out on Applied Biosystems StepOnePlus PCR system. mRNA fold change were determined using the $2^{-\Delta\Delta C_T}$ method and statistical analysis were performed using GraphPad Prism software.

2.6: DEVICE FABRICATION
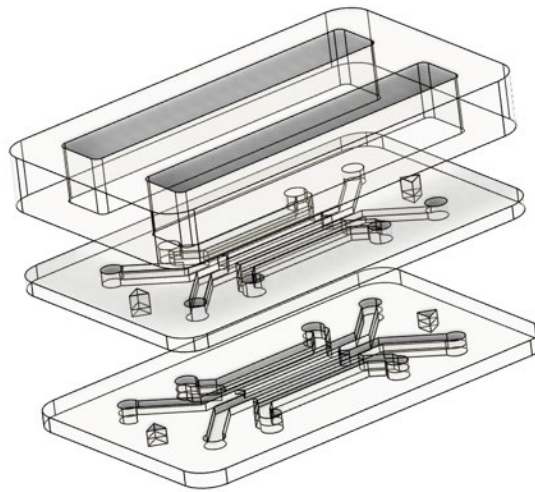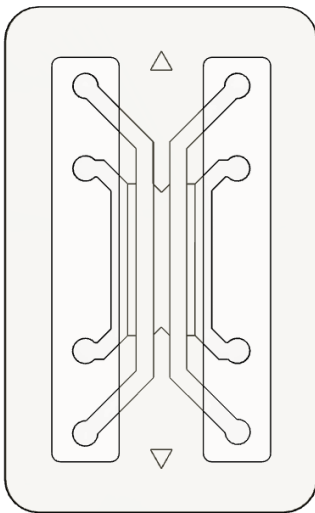
Figure 6: Double lane, membrane-free organ chip device schematic

Clear resin molds were designed in Fusion360 and 3D printed using FormLabs Form 3B printer. Resin molds were then washed with isopropyl alcohol (IPA) three times for 20 minutes each using FormLabs Wash before being cured at 60ºC for 20 minutes with FormLabs Cure. The curing process typically results in slight warping of resin molds. To address this, while also removing volatiles, resin molds were baked at 130ºC for 2 hours and then immediately sandwiched between two 130ºC jewelers blocks overnight to flatten molds.

Double lane, membrane-free organ chips were fabricated by using polydimethylsiloxane (PDMS) elastomer (Sylgard) in a 1:10 ratio of curing agent to elastomer. After PDMS was degassed, PDMS was poured onto molds and degassed before being baked at 60ºC for 12 hours. After PDMS cured, layers were bonded using spin coated PDMS on a Petri dish and allowed to dry for 24 hours. Following bonding, devices were sterilized via ultraviolet (UV) for 30 minutes before polydopamine (PDA) treatment. Vascular gel channels were treated with 5mg/mL PDA (Sigma Aldrich) for 3 hours with UV and then washed with ultrapure distilled water twice.

2.7: VASCULAR GEL

Vascular gel was prepared using HUVECs (density: 2×10^6 cells/mL), HLFs (density: 2×10^6 cells/mL), 10X DMEM (DMEM:Final Volume = 75:1000), 1M NaOH (NaOH:DMEM = 1:2.5), collagen type I rat tail (final concentration: 2.2mg/mL), fibrinogen (final concentration: 5mg/mL), and thrombin (Thrombin:Final Volume = 1:100). Vascular gel was maintained for a total of 10 days with media changes using VEGM media without VEGF every other day.

28

2.8: FLOW CYTOMETRY

Media was collected in the middle of cisplatin treatment to collect floating dead cells in suspension, as well as at end point. At end point, cells were washed with 1mL sterile phosphate buffer saline and then trypsinized with 0.05% trypsin-EDTA and incubated at 37ºC for 6 minutes. Then trypsinization was blocked with 2mL media and then contents were collected for centrifugation at 1000 rpm for 5 minutes. Cells were resuspended in 2mL non-sterile PBS and then split into 2 flow cytometry tubes with 1mL each. One tube was used as an unstained control and another tube was stained with DAPI at a 1:1000 dilution. Samples were centrifuged at 1000 rpm for 5 minutes and then resuspended in 500uL non-sterile PBS.

Table 2: Flow Cytometry Voltages			
	FSC	SSC	V450
Voltage	682	268	429

Flow cytometry was carried out using FACS Melody. Data was analyzed using FlowJo software. First forward scatter plot and side scatter plots were gated to exclude cell debris and doublets. This gated area represents the singlet cell population. Then this gated area was used to produce a plot of V450, for DAPI, versus side scatter. On this plot, three populations – Late Dead, Early Dead, and Live – were quantified based on relative cell size and permeability to DAPI. DAPI stains to the minor grooves of DNA in a concentration dependent manner. This means that DAPI can bind to smaller cells with more permeable membranes as opposed to larger cells with normal membrane permeability. Late Dead population is highly permeable to DAPI and its signal is higher than the Live population. Early Dead population is also permeable to DAPI but is larger

29

in size than Late Dead. Live population is not as permeable to DAPI as Early Dead and Late

Dead populations but Live cell size is larger than Late Dead.
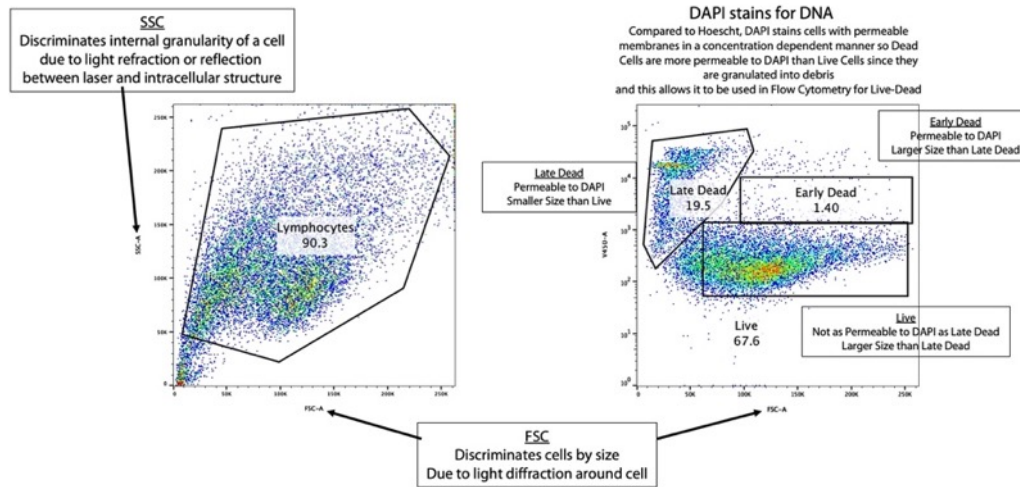
Figure 7: Defining parameters of various populations evident in flow cytometry: Late Dead,

Early Dead, and Live

2.9: CRYSTAL VIOLET

Cells were seeded at 1,000 cells/well and cultured in a 96 well plate until confluency, at which

point they underwent our cisplatin treatment regimen. Following the treatment regimen, cells

were fixed in 4% paraformaldehyde for 15 minutes and washed with Dulbeccos phosphate buffer

solution (DPBS, Corning) prior to staining. Crystal violet (CV) solution (Sigma Aldrich V5265)

was made at 1:10 in 10% methanol. The CV solution was added to the plate and incubated for 30

minutes at room temperature. Cells were washed with DPBS until the solution ran clear and set

30

to dry overnight. Crystal violet was eluted with 33% acetic acid solution and read on a plate reader at 570nm.

2.10: IMMUNOHISTOCHEMICAL STAINING

Cell monolayers were seeded at 30,000 cells per well and cultured for 4 days. Monolayers were fixed in 4% PFA for 15 minutes and washed with DPBS prior to immunostaining. Samples were blocked and permeabilized for 20 minutes in 1% bovine serum albumin (BSA) and 0.1% Triton-X, prepared in DPBS. Primary Ki-67 antibody (Rabbit polyclonal to Ki67 [abcam ab15580]), smooth muscle actin (Mouse monoclonal to alpha smooth muscle actin [abcam ab7817]), PRRX1 (Rabbit polyclonal to PRRX1 [Invitrogen PA5-106700]), and Gli1 (Mouse monoclonal to Gli1 [Santa Cruz sc-515751]) was added at 1:100 in 0.1% BSA prepared in DPBS and incubated at room temperature for 2 hours with gentle rocking. Primary active YAP1 (rabbit monoclonal to active YAP1 [abcam ab205270]) was added at 1:200. Samples were washed with DPBS and then secondary antibody (Alexafluor 488 donkey anti mouse IgG [abcam ab150105], Alexafluor 594 goat anti rabbit IgG [abcam 150080]), Hoescht 33432 [62249, Thermo Scientific 62249]) and phalloidin was added at 1:500 in 0.1% BSA prepared in DPBS and incubated in the dark for 1 hour with gentle rocking. Samples were washed with DPBS before confocal imaging. After 5 days in culture, spheroids were washed with non-sterile PBS and then fixed in 4% paraformaldehyde for 24 hours at 2ºC. After fixing, spheroids were washed with three times over 10 minutes with non-sterile PBS and then blocked and permeabilized in 3% bovine serum albumin and 0.05% Triton-X, prepared in PBS, for 30 minutes. Then spheroids were incubated with Ki67 primary antibody for 1 hour at room temperature and then placed in 2ºC for 18 hours.

31

After primary antibody incubation, spheroids were washed five times over 1 hour with non-sterile PBS. Spheroids were then incubated with secondary antibodies Hoescht 33432, Ki67 and Phalloidin for 1 hour at room temperature. Afterwards, spheroids were washed four times over 30 minutes at which point spheroids are ready to be imaged.

At endpoint, vascular gels were fixed with 4% paraformaldehyde (PFA) for 1 hour at room temperature, and then 12 hours at 4ºC. After washing PFA three times over 15 minutes, Hoescht 33432 (1:250), Phalloidin 488 (1:250), and Human Lectin UEA (1:100) in 1% bovine serum albumin and 0.2% Triton-X solution for 1 hour at room temperature on rocker and then 12 hours at 4ºC. After staining, vascular gels were washed five times with PBS over 3 hours on rocker.

2.11: CONFOCAL IMAGING

Samples were imaged in their respective plates using a Nikon Ti-2 Confocal Microscope at 10x objective on DAPI, FITC, and TRITC channels. All images were acquired using the same settings and images were denoised using Nikon's proprietary software prior to image analysis. Specific image acquisition methods are mentioned within the appropriate subsections of these methods.

2.12: Ki67, SPHEROID MORPHOLOGICAL, 2D MORPHOLOGY IMAGE ANALYSIS

Ki67 quantification, spheroid morphology and 2D morphology were conducted using open-source CellProfiler (Broad Institute, Cambridge, MA, USA) and project pipelines employed are available for public download at http://www.github.com/omarmkahmad/mse. Briefly, 20 slices in the Z-projection were captured for each spheroid with the top and bottom of the spheroid being identified using the FITC channel for phalloidin staining. After capturing images, MAX

32

intensity z-projections were made using ImageJ before importing into CellProfiler. CellProfiler outputted Solidity, Compactness, Form Factor, and Area metrics. Solidity is defined as The proportion of the pixels in the convex hull that are also in the object, i.e., ObjectArea/ConvexHullArea. Compactness is defined as $Perimeter^2/4*\pi*Area$, related to Form Factor. A filled circle will have a compactness of 1, with irregular objects or objects with holes having a value greater than 1. Form Factor is defined as $4*\pi*Area/Perimeter^2$ and equals 1 for a perfectly circular object. The Area of the 2D max projected slice was also obtained to represent the cross-sectional area.

2.13: ANGIOGENESIS IMAGE ANALYSIS

Stained vascular gels were placed on glass slide and imaged on inverted Nikon C2 laser scanning confocal microscope equipped with Nikon DS-FI3 camera. A 6x1 stitched z-stack of each vascular gel was captured. Max intensity projection of z-stacks were initially denoised using Nikon's proprietary denoise function and then exported as TIFFs for image analysis. Image analysis was conducted in MATLAB (R2021b). First, vascular network images were smoothed using an edge-preserving filter with a Gaussian kernel, and a threshold was applied to remove the remaining low-intensity noise. We then used a pretrained deep neural network from MATLAB's Deep Learning toolbox to denoise each image, followed by use of adaptive histogram equalization to standardize contrast across the image set. Following this, we segmented pre-processed images and quantified morphometric parameters using an open-source automated segmentation tool (REAVER). For quantification of angiogenic sprout growth, DIC images of the central channel of each chip were used to identify the boundary between the cancer spheroid

33

and vascular channel, and morphometric quantification was performed on the region of interest, bound by the gel interface and the tip of each sprout in the cancer spheroid channel.

2.14: STATISTICAL ANALYSIS

All statistical analysis were performed using GraphPad Prism version 9.2.0 for Mac, GraphPad, Software, San Diego, California, USA www.graphpad.com.

2.14A: CELL SURVIVAL

Ordinary one-way ANOVA with Dunnett's multiple comparison test, using normalized parental A549 as control, was performed for % cell survival analysis.

2.14B: 2D MORPHOLOGICAL ANALYSIS OF 2D AND 3D TISSUES

Paired t-test between parent and cisplatin-resistant tissues were performed for analysis of nuclear and cellular area and diameter.

2.14C: KI67 INDEX

Paired t-test between parent and cisplatin-resistant tissues were performed for analysis of Ki67 index.

2.14D: MRNA GENETIC EXPRESSION

Ordinary one-way ANOVA with Dunnett's multiple comparison test, using parental A549 as control, was performed for analysis of mRNA fold change.

2.14E: ANGIOGENIC SPROUTING

Unpaired t-test of Vessel Area, Vessel Density, and Vessel Length was performed for analysis of varying parameters of angiogenic sprouting.

34

CHAPTER 3: RESULTS

3.1: CYTOTOXICITY DOSE RESPONSE ASSESSMENT BY FLOW CYTOMETRY

A549 lung adenocarcinoma cells treated with cisplatin over 96 hours, across two 48 hour

intervals, yield cells that are more mesenchymal-like in morphology (Figure 8). This likely

indicates that they are undergoing the epithelial-to-mesenchymal transition.

Across all populations of cisplatin concentration, A549s morphology varied.
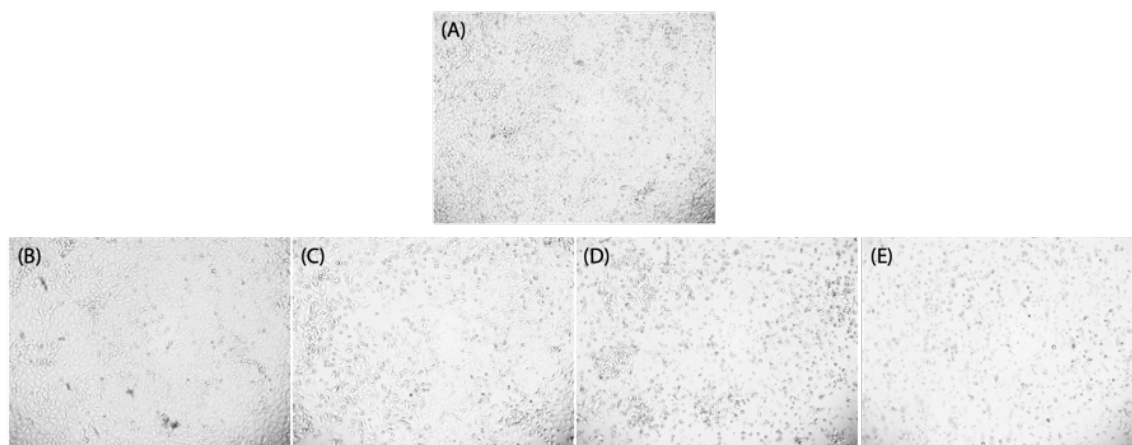
Figure 8: A549 lung adenocarcinoma cells after 96 hour cisplatin treatment. (A) Parent
A549s untreated. (B) A549s treated with 15uM. (C) A549s treated with 25uM. (D)
A549s treated with 35uM. (D) A549s treated with 45uM.

In 15uM population (Figure 8.B), A549s appear to maintain their epithelial morphology.

However, in the 25uM (Figure 8.C) and 35uM populations (Figure 8.D), A549s start to show a

more mesenchymal-like morphology. However, differences in the 25uM and 35uM populations

show that 35uM also start to die more than the 25uM population, as indicated by the small

circular cells. Moreover, in the 45uM population (Figure 8.E), A549s appear to mainly die from

such a high concentration of cisplatin. Therefore, 25uM was closely investigated based off these

observations.
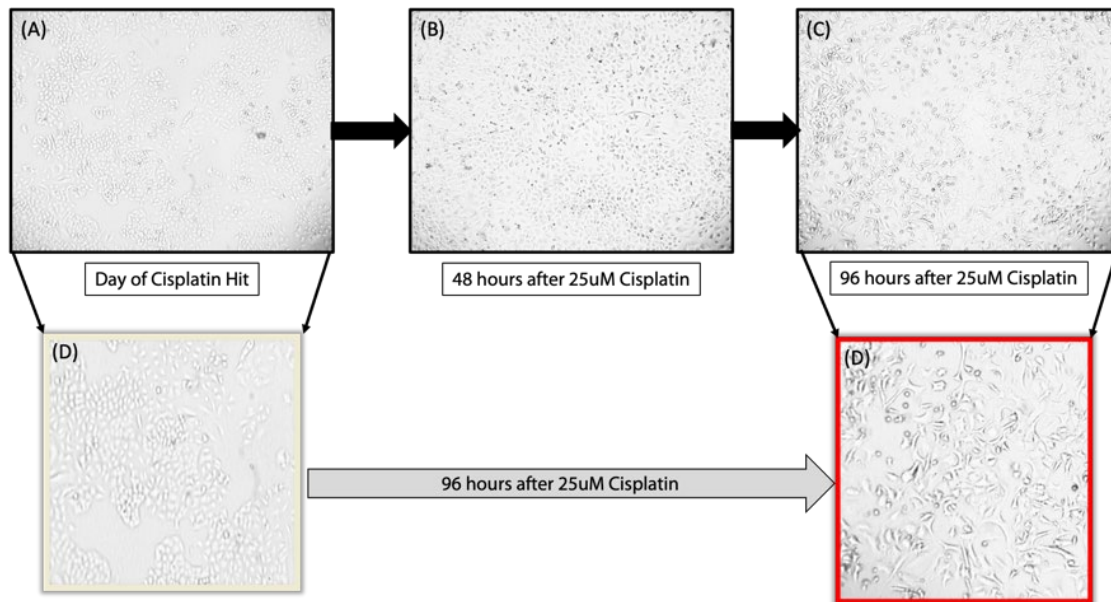
Figure 9: Morphological changes in A549s treated with 25uM cisplatin across 96 hour treatment. (A) A549s covering approximately 70% of T25 surface area on the day of first cisplatin hit. (B) A549s after 48 hours from first cisplatin hit and day of second cisplatin hit. (C) A549s after 96 hours from initial cisplatin hit (48 hours after second cisplatin hit). (D) 20x magnification view of A549s covering approximately 70% of T25 surface area on the day of first cisplatin hit. (E) 20x magnification view of A549s after 96 hours from initial cisplatin hit.

Figure 9.D shows that A549s treated with 25uM cisplatin over 96 hours appear mesenchymal in

morphology. This mesenchymal morphology was not evident after the first drug hit (Figure 9.B)

rather they still maintain an epithelial morphology. Therefore the morphological transition from

epithelial to mesenchymal morphology likely occurs between 48 hours and 96 hours.

36
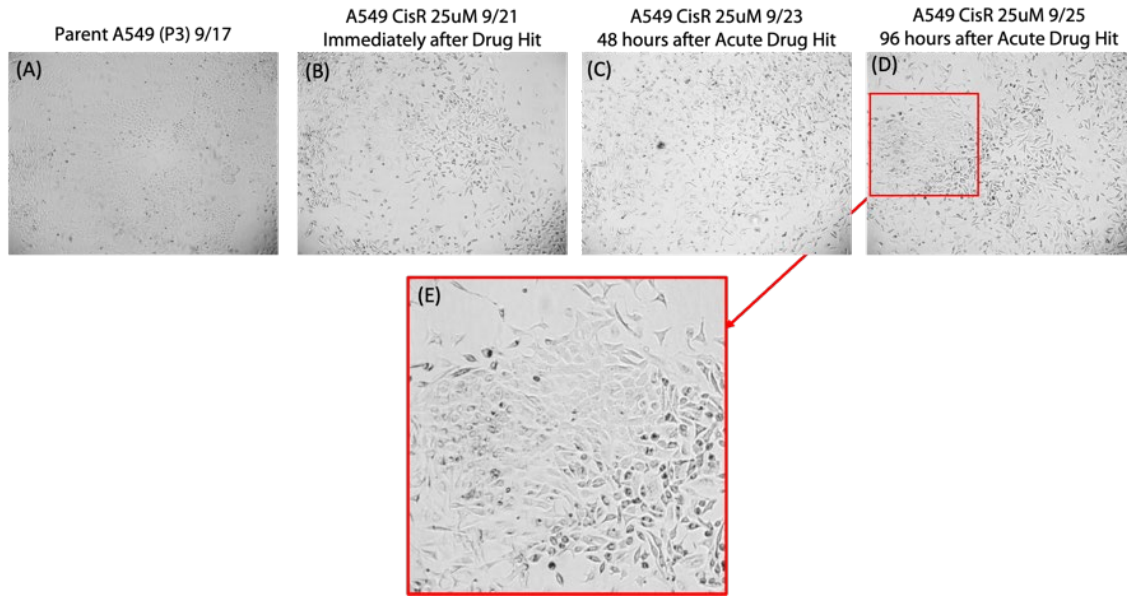
Figure 10: Rise of rapidly proliferating small cell morphology after 96 hour 25uM cisplatin treatment in A549s.

In addition to mesenchymal-like cells arising, rapidly proliferating smaller cells (Figure 10.E) also appear to arise in 25uM population after 96 hours. These smaller cell populations appear to join together and form a border of mesenchymal cells surrounding a smaller cell core.

37
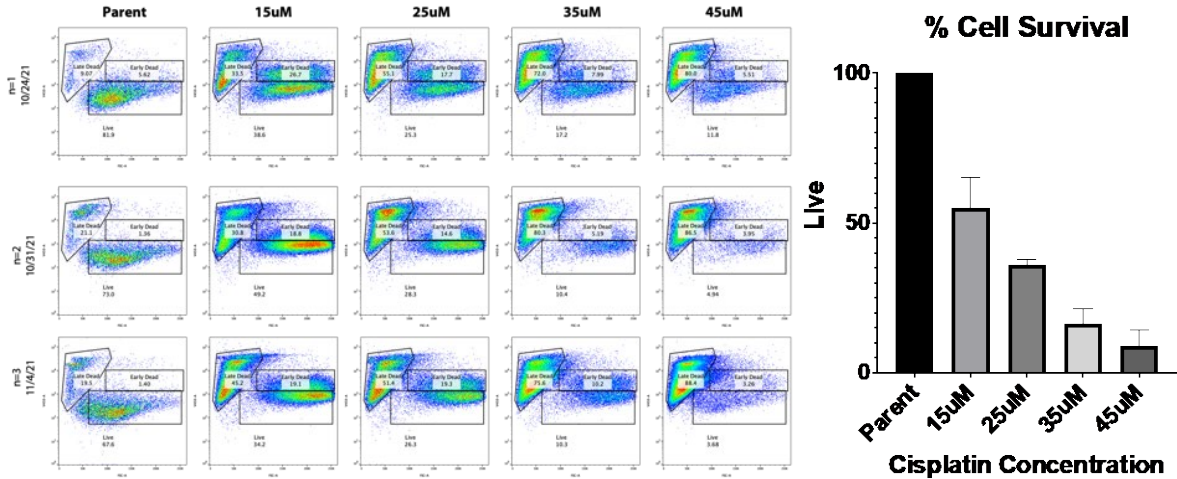
Figure 11: Flow Cytometry data from 2D cultures of Parent, 15uM, 25uM, 35uM, and 45uM CisR A549s. <u>Late Dead</u>: Permeable to DAPI and Smaller Size than Live. <u>Early Dead</u>: Permeable to DAPI and Larger Size than Late Dead. <u>Live</u>: Not as Permeable to DAPI as Late Dead. Larger Size than Late Dead.

To validate cell survival from cisplatin administration, Flow Cytometry (Figure 11) was conducted with DAPI staining at end point across n = 3 trials, consistent with the aforementioned cisplatin treatment regimen. Parent population yielded 74.16% cell survival whereas 15uM yielded 54.83%, 25uM yielded 35.91%, 35uM yielded 16.51%, and 45uM yielded 8.86% (Figure 11). 25uM cell survival is the closest population to half of parental population.

3.2: CYTOTOXICITY DOSE RESPONSE ASSESSMENT BY CRYSTAL VIOLET

Further validation of cell survival was validated using crystal violet staining (Figure 12). CV staining revealed similar trends in cell survival as flow cytometric analysis. 5uM population yielded 79.64% cell survival; 15uM population yielded 58.98% cell survival; 25uM population yielded 22.91% cell survival; 35uM population yielded 6.978% cell survival; 45uM population yielded 7.438% cell survival; and 55uM population yielded 7.358% cell survival.

38
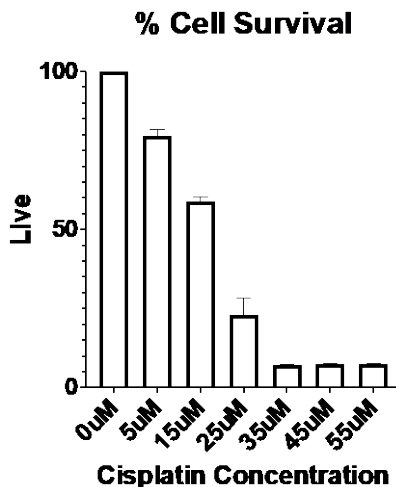
Figure 12: Crystal violet staining from 2D cultures of Parent, 5uM, 15uM, 25uM, 35uM, 45uM, and 55uM CisR A549s.

3.3: 2D MORPHOLOGY OF CISPLATIN-RESISTANT TISSUES

Following cisplatin dose validation, 2D morphology of cisplatin-resistant A549s were analyzed

using Hoescht 33432, Phalloidin, and Ki67 immunostaining to assess cellular and nuclear area

and diameter (Figure 13). Phalloidin stains for filamentous actin (F-actin), an essential

cytoskeletal component in eukaryotic cells[71]. Ki67 is a nuclear protein associated with cellular

proliferation and is widely used in clinics to assess tumor aggressivity[72]. Higher Ki67 expression

often correlates with more aggressive tumor behavior and poorer clinical outcomes[72]. Cisplatin-

resistant tissues revealed drastically larger cellular and nuclear area and diameter (n=, $p < 0.0001$)

relative to parent tissues (Table 3). Additionally, cisplatin-resistant tissues had reduced Ki67

expression relative to parent A549 tissues (Figure 14).

39
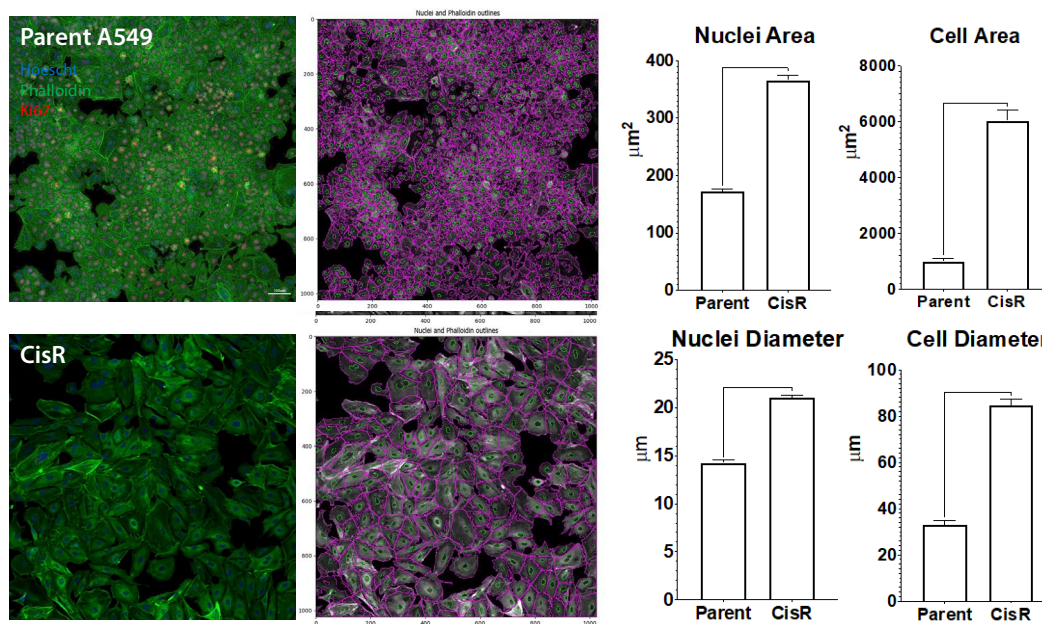
Figure 13: 2D morphology of parental and cisplatin-resistant A549 lung adenocarcinoma cells. Scale bar = 100um

	Parent A549	Cisplatin-Resistant A549s
Nuclei Area (um^2)	171.75	366.06
Nuclei Diameter (um)	14.26	21.00
Cell Area (um^2)	999.04	6034.91
Cell Diameter (um)	33.14	84.61

Table 3: Morphological results of parental and cisplatin-resistant A549 lung adenocarcinoma cells
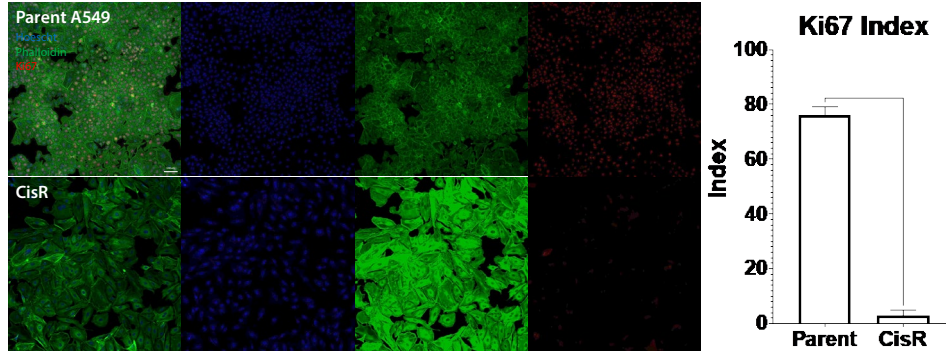
Figure 14: Ki67 index of 2D parental and cisplatin-resistant A549 lung adenocarcinoma cells. Scale bar = 100um

This increase in cellular area could be attributed to senescence, wherein after insulting DNA repair mechanisms with cisplatin, cells can grow too large[73].

3.4: 3D MORPHOLOGY OF CISPLATIN-RESISTANT TISSUES

These results translated to the 3D tumor spheroids where Ki67 expression was lower in cisplatin-resistant A549s relative to parent A549 spheroids (Figure 15).
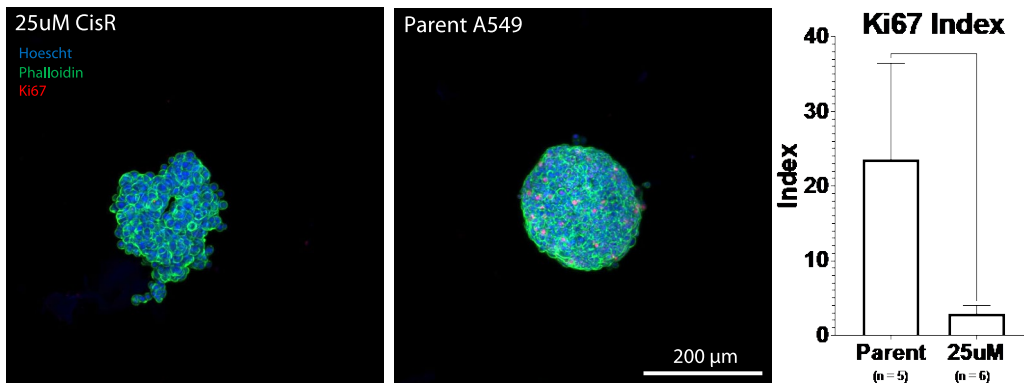
Figure 15: Ki67 index of parental and cisplatin-resistant A549 lung adenocarcinoma spheroids. Scale bar = 200um.

Interestingly, cisplatin-resistant spheroids developed a dysmorphic morphology relative to the

nearly spherical parent spheroids (Figure 16).
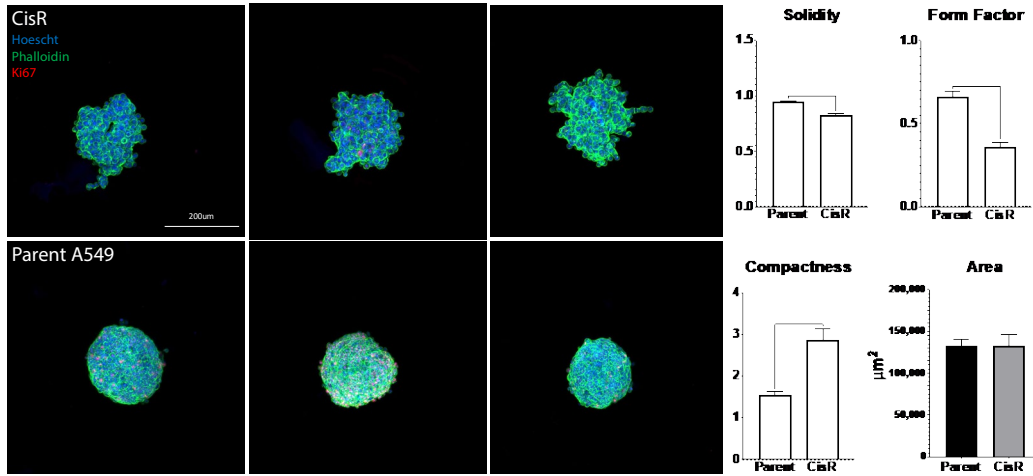
Figure 16: 3D morphology of parental and cisplatin-resistant A549 lung adenocarcinoma
spheroids. Scale bar = 200um

3.5: GENETIC EXPRESSION OF CISPLATIN-RESISTANT TISSUES

To elucidate the genetic underpinnings of these morphological changes, we quantified mRNA

fold changes in a variety of genes implicated in cisplatin resistance and EMT. Additionally, we

wanted to investigate the existence of any temporal factors following cisplatin administration

that influenced chemoresistance. Therefore, we defined two populations – post-treatment and

endpoint – to collect RNA (Figure 17). Post-treatment refers to tissues collected immediately

following the 96 hour treatment regimen, whereas Endpoint refers to tissues collected at

timepoint for functional assays.

42
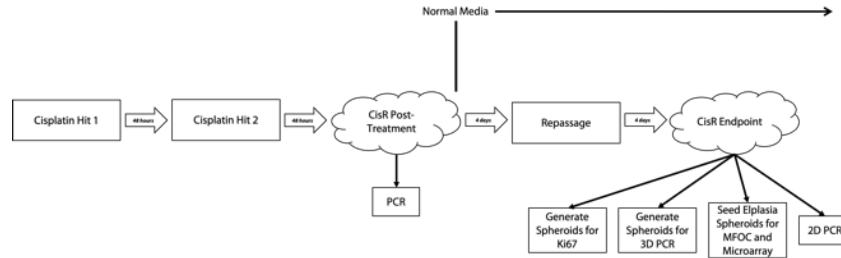
Figure 17: Collection of post-treatment and endpoint cisplatin-resistant tissues

VEGFA expression was slightly downregulated (fold change = 0.75 ± 0.21) post-treatment and was upregulated at endpoint (fold change = 1.12 ± 0.90) relative to parent. *IL8* (Interleukin-8) is associated with chemoresistance by promoting angiogenesis and inflammation in the tumor microenvironment in lung adenocarcinoma[74]. We found an upregulation of *IL8* in both post-treatment (fold change = 10.21 ± 6.84) and endpoint (fold change = 8.89 ± 8.19) tissues. *aSMA* (alpha-smooth muscle actin) upregulation has been associated with an aggressive phenotype and poorer prognosis, as well as chemoresistance, in lung adenocarcinoma[75]. *aSMA* was upregulated relatively consistently in both post-treatment (fold change = 8.37 ± 0.99) and endpoint (fold change = 8.35 ± 1.18) tissues. E-cadherin (*CDH1*) is a critical cell adhesion molecule and its downregulation is implicated in EMT, which is said to lead to chemoresistance in lung adenocarcinoma tissues[54]. CDH1 was upregulated at both timepoints with a markedly higher expression at endpoint (fold change = 1.56 ± 0.33) relative to post-treatment (fold change = 1.89 ± 0.58).

43
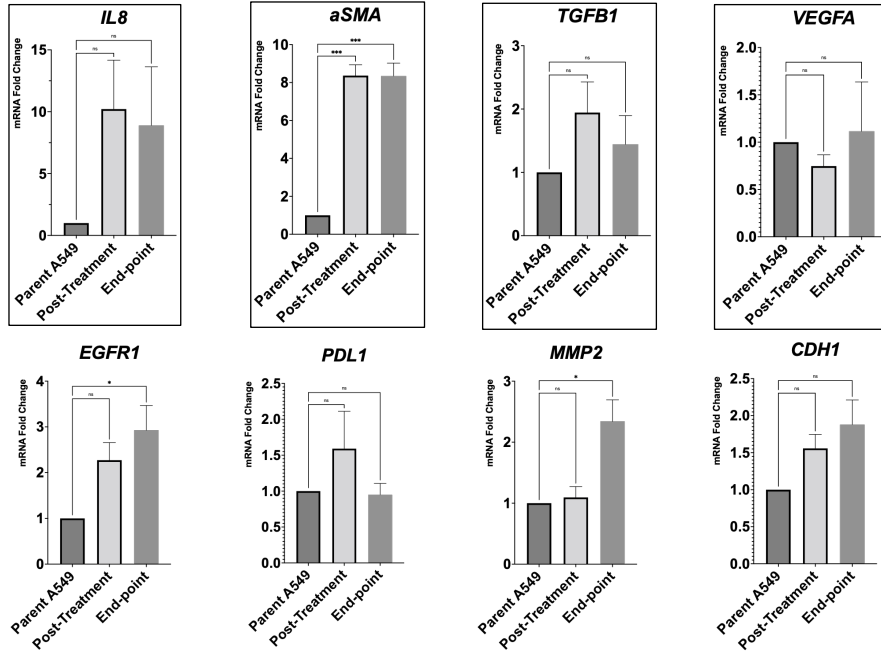
Figure 18: mRNA genetic expression panel of post-treatment and endpoint cisplatin-resistant A549 lung adenocarcinoma tissues

TGFB1 (transforming growth factor receptor beta 1) is known for promoting EMT in lung adenocarcinoma and its upregulation is also linked to cisplatin resistance in lung adenocarcinoma[76]. *TGFB1* expression was upregulated at both timepoints (post-treatment fold change = 1.56 ± 0.33; endpoint fold change = 1.88 ± 0.58) relative to parent A549s. *EGFR1* (epidermal growth factor receptor 1) is involved in cellular proliferation and is linked to cisplatin resistance in NSCLC[77]. *EGFR1* expression at endpoint (fold change = 2.93 ± 0.94) was slightly higher than post-treatment (fold change = 2.27 ± 0.67). *PDL1* (programmed death-ligand 1) expression within tumor cells can lead to immune evasion and has been associated with chemoresistance in lung adenocarcinoma[78]. *PDL1* expression post treatment was upregulated (fold change = 1.59 ± 0.90) but was down regulated at endpoint (fold change = 0.95 ± 0.27).

44

MMP2 (matrix metalloproteinase 2) is involved in the degradation and remodeling of lung adenocarcinoma ECM, thereby promoting tumor invasion and metastasis and its upregulation has been implicated in cisplatin resistance in lung adenocarcinoma[79]. MMP2 expression post-treatment was slightly upregulated (fold change = 1.09 ± 0.31) and further upregulated at endpoint (2.34 ± 0.61).
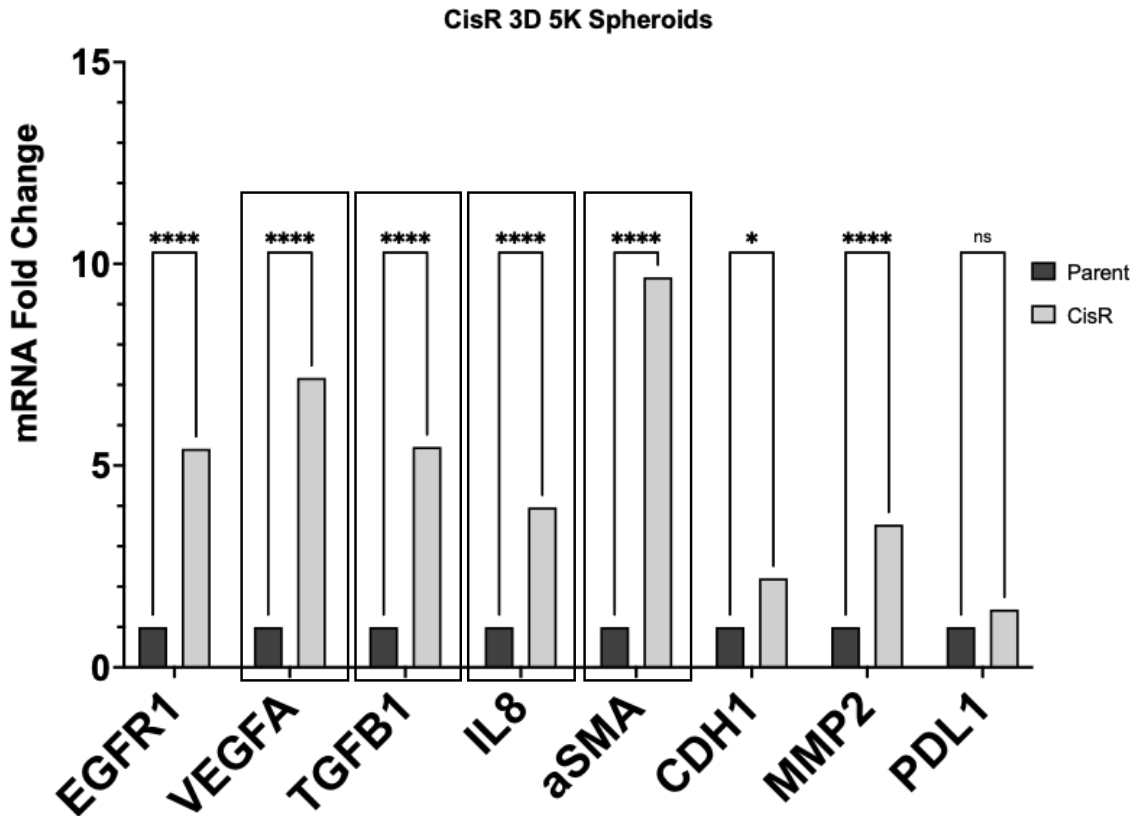
Figure 19: mRNA genetic expression panel of 3D parental A549 and CisR A549 spheroids mRNA expression in cisplatin-resistant spheroids largely resembled that of 2D tissues with an exception for *VEGFA*, which had a high upregulation in cisplatin-resistant spheroids (fold

change = 7.17 ± 1.69) relative to parent spheroids. This is in stark contrast to 2D PCR data on the same tissues which had subtle differences in *VEGFA*.

3.6: ANGIOGENIC SPROUTING OF CISPLATIN-RESISTANT TISSUES
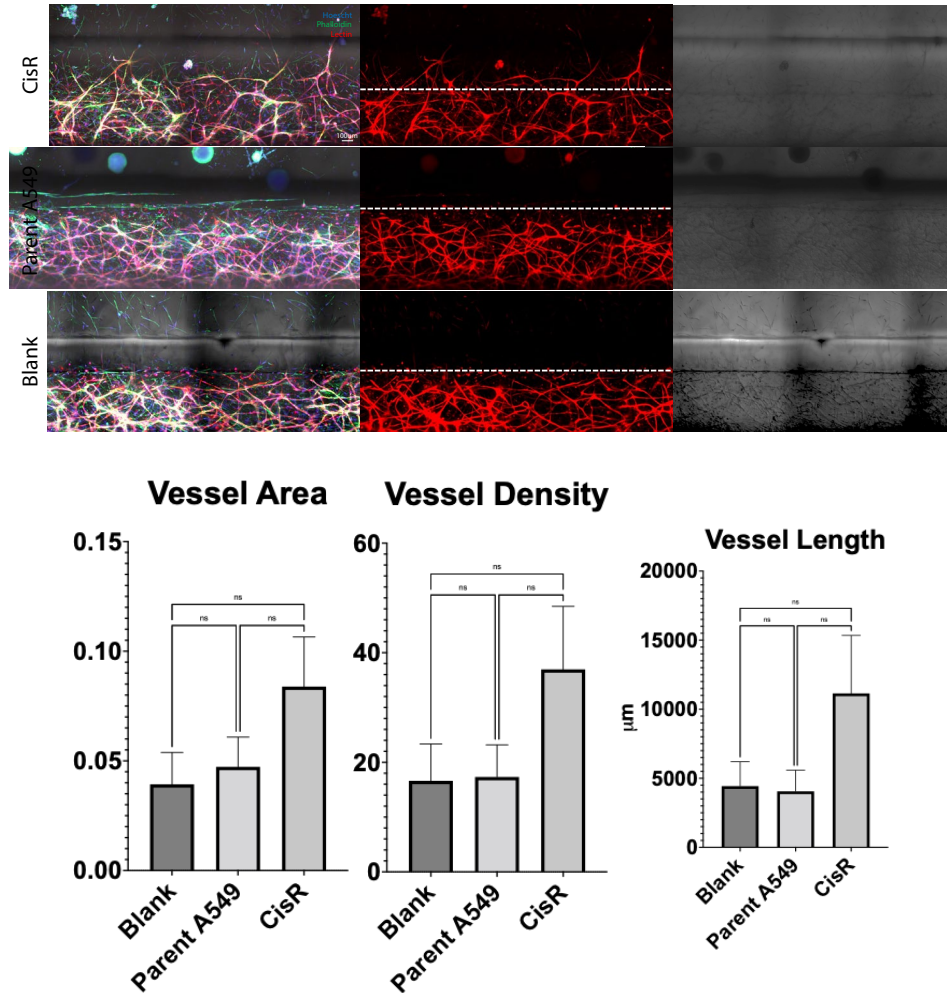
Figure 20: Cisplatin resistant A549s reveal more angiogenic sprouting, relative to parental A549s, evident by increased vessel area, vessel length, and vessel density in double lane membrane-free organ chip. Scale bar = 100um.

This increased expression of *VEGFA* motivated us to investigate angiogenic sprouting in our vascularized double lane membrane-free organ chips. Herein, we found that cisplatin -resistant

46

tissues exhibited more angiogenic sprouting relative to parent A549s when assessing vessel area

(CisR = 0.083, parent = 0.047, blank = 0.039), vessel length (CisR = 11143.4um, parent =

4065.2um, and blank = 4433.75um), and vessel density (CisR = 36.96, parent = 17.32, and blank

= 16.62).

3.7: GENETIC EXPRESSION AND ANGIOGENIC SPROUTING OF ERK5-/- TISSUES
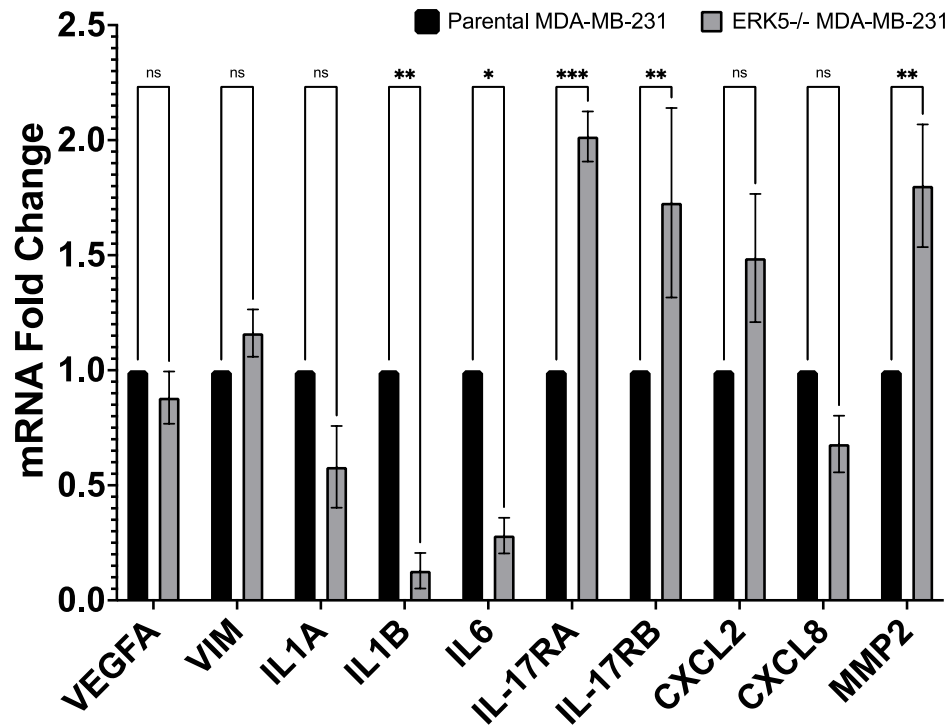
Figure 21: mRNA genetic expression panel for parental and ERK5-/- MBA-MB-231 tissues
We then attempted to expand this outside of cisplatin-resistance in NSCLC to TNBC.
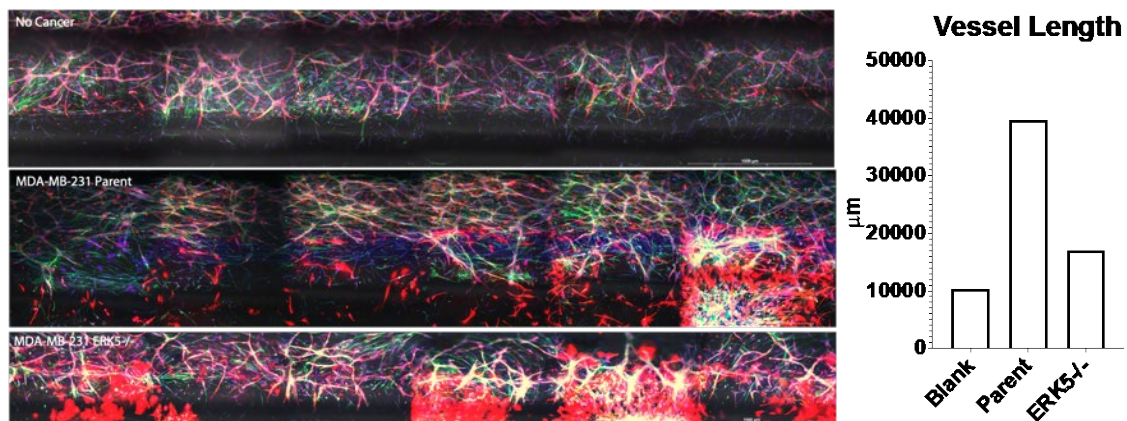
Figure 22: ERK5-/- tissues reveal reduced vessel length, relative to parental MDA-MB-231 tissues in double lane membrane-free organ chip device. Scale bar = 1000um.

We corroborated existing work from collaborators work showing that ERK5-/- in MDA-MB-231

tissues reveals reduced angiogenic development relative to parental MDA-MB-231 tissues.

48

CHAPTER 4: DISCUSSION

4.1: Generation of Cisplatin Resistant Lung Adenocarcinoma Tissues

In this study, we successfully generated cisplatin-resistant lung adenocarcinoma from parental cell line A549 by leveraging a 96 hour drug treatment. Briefly, parental A549s were grown to near confluency at which point they were exposed to cisplatin doses for 48 hour increments for a total of 96 hours. The selection of 25uM as the appropriate cisplatin dose was based on flow cytometry and crystal violet analysis which revealed a 35.91% recovery relative to parental population yielding 74.16% cell survival (Figure 11). Previous work characterizing and generating cisplatin-resistant A549s have found similar percent proliferation for cisplatin dosing as our work; however, it is important to note that treatment times varied in these other protocols[80,81]. The initial advantage of our shorter drug protocol, relative to weeks and months long protocols, is to provide a higher throughput approach to recapitulating cisplatin-resistance *in vitro* for use in organs-on-a-chip. While long-term treatment protocols may allow for the investigation of more "stable" features of cisplatin resistance (i.e., cellular import and export of cisplatin), the increased exposure time allows for more genetic mutations to develop which moves away from physiological relevance of cisplatin treatment in the clinic. Previously described disadvantages of shorter term cisplatin resistant protocols mainly highlight how molecular changes are smaller and less discernable; however, it is our hope that genetic sequencing approaches coupled with multi-organ chips can help discern these molecular changes in short-term, physiologically similar cisplatin treatment regimens.

49

Our findings revealed that our cisplatin-resistant tissues displayed a larger cellular and nuclear area and diameter relative to parental A549s (Figure 13). Previous work describing alterations in cellular growth as a result of cisplatin-resistance also demonstrated that cisplatin-resistant tissues adopt mesenchymal characteristics, including increased CDH1 (E-cadherin) and TGFB1[17,82]. In these findings, researchers have attributed this to changes that occur during EMT. Changes in cytoskeletal organization of these parental epithelial-type cells lead to a more elongated morphology, which we show in Figure 10[17]. Accompanying this is a resistance to apoptosis in the cisplatin-resistant tissues, which leads to an increase in cell size due to the accumulation of cellular components, as well as an increase in nuclear area as a result of changes in chromatin organization[17]. Furthermore, this also culminates into changes in cell cycle alterations when cells are spending more of their time in G1 (during which cellular and nuclear components are being synthesized), resulting in increases in cellular and nuclear sizes. This is corroborated by work specifically into the distribution of cisplatin-resistant A549s in differing phases of the cell cycle, which found a significant portion of cisplatin-resistant A549 cells remain in G1, relative to parental A549s, when compared to other phases of the cell cycle[80] (Figure 23).

50
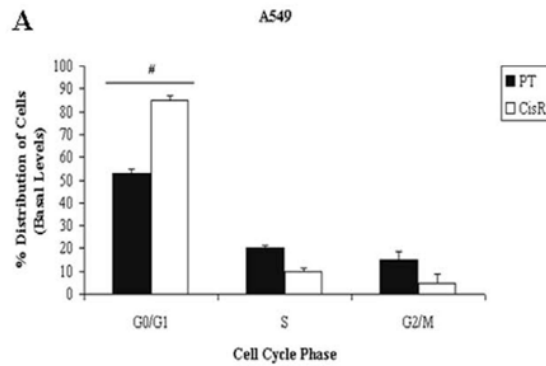
Figure 23: Cisplatin-resistant cells accumulate in the G1 phase of the cell cycles (Galluzzi 2013)

This is where we decided to investigate the genetic expression of various genes implicated in EMT and inflammation for both 2D and 3D cisplatin-resistant tissues (Figure 18). Our results from *TGFB1*, *EGFR*, and *CDH1* mRNA expression in 2D cisplatin-resistant A549s are in line with previous bodies of work discussing EMT related genes[83–85]. Our work expanded upon extensive bodies of work by characterizing the differential expression in 3D tumor spheroids (Figure 24). This is critical considering tumor spheroids are more physiologically relevant tissue models of tumors in vivo for their ability to replicate complex cell-cell interactions that are not evident in 2D monolayers[86].

mRNA Fold Changes 2D vs 3D		
Gene	2D	3D Spheroid
VEGFA	1.1	7.2
TGFB1	1.5	5.5
aSMA	8.4	9.7
IL8	8.9	3.4
PDL1	0.9	1.4
MMP2	2.4	3.6
EGFR1	2.9	5.4
CDH1	1.9	2.1

Figure 24: Summary of differing mRNA fold changes for various genes implicated in EMT, inflammation, and angiogenesis in cisplatin-resistant lung adenocarcinoma

Of note are the changes in *VEGFA* expression (1.1 vs 7.2), *TGFB1* expression (1.5 to 5.5), and *IL8* expression (8.9 to 3.4).

In both 2D and 3D, we found our cisplatin-resistant A549s had a significant decrease in Ki67 index (2D = 2.9; 3D = 2.8) relative to parental A549s (Figure 14 and 15). Other work[80] describing decreased proliferative potential of cisplatin-resistant A549s relative to parental A549s after 1 year aligns with our shorter treatment protocol highlighting reduced proliferative capacity. Previous work[80] attributes this reduced proliferation in cisplatin-resistant tissues to DNA damage; however, we expand upon this explanation to claim that aggressivity is not solely defined by Ki67 index, but also by the resistant tissue's enhanced invasive and migration capacity. This can be explained both by an adoption of a mesenchymal phenotype at the end of EMT. Unfortunately, no work at the time of publishing this describes microphysiological system models being leveraged for characterizing EMT in the context of drug resistance. Therefore, we decided to leverage our double lane membrane-free organ chip for angiogenic sprouting to investigate EMT in the context of cisplatin-resistance. In Figure 20, we showed that cisplatin-

52

resistant tissues exhibit more angiogenic sprouting relative to parental A549s. Angiogenic sprouting gives way for resistant tumor cells to disseminate from the primary tumor site and travel to distant organs to initiate metastasis[87]. It is well established that increased metastasis is a critical hurdle for later stage NSCLC patients to grapple with as standard, first-line cisplatin therapy often fails leading to roughly 30-55% of NSCLC cases recurring[11]. To the best of our knowledge, a limited body of work exists that directly investigates angiogenic sprouting in cisplatin-resistant lung adenocarcinoma; however, work discussing the role of a certain microRNA (miR-93-5p) contributing to the angiogenic capabilities of cisplatin-resistant NSCLC by targeting the expression of specific inhibitors has been studied[88].

Future work into generating more physiologically relevant models of lung adenocarcinoma cisplatin-resistance may look specifically at how anti-angiogenic therapies can be optimized in conjunction with first-line cisplatin treatment to prevent tumor recurrence.

4.2: Translation to ERK5-/- Triple-Negative Breast Cancer Tissues

We wanted to apply our approach with the cisplatin-resistant lung adenocarcinoma tissues to another global leading type of cancer, triple-negative breast cancer. Our collaborators have recently shown that CRISPR/Cas9 deletion of the *ERK5* gene in triple-negative breast cancer cell line MDA-MB-231 suppresses angiogenesis in tumor xenografts from mouse models[40]. Little has been reported on *ERK5*'s role in TNBC as its role has only recently been implicated; however, its proposed role in TNBC is said to mediate breast tumor formation through both cell intrinsic and extrinsic mechanisms by promoting EMT and pro-angiogenic growth factors.

53
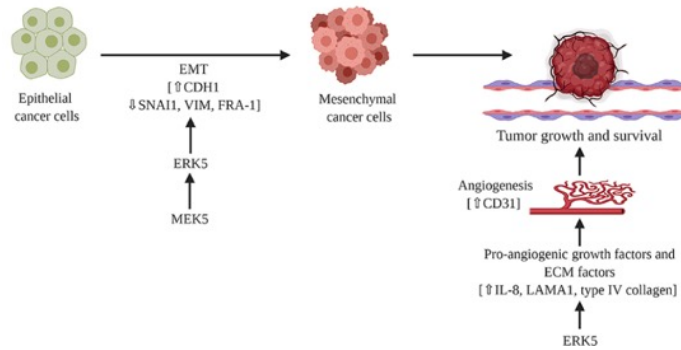
Figure 25: Proposed mechanism for *ERK5*'s role in TNBC (Hoang 2020)

Our objective was to corroborate data showing that *ERK5-/-* tumors exhibit less angiogenic sprouting than parental MDA-MB-231 tumors. We first started by characterizing the mRNA genetic expression of both *ERK5-/-* and MDA-MB-231 tissues across subsequent passages for various EMT and inflammatory genes (Figure 21).

Interestingly, we found that, similar to with the cisplatin-resistant tissues in 2D, *ERK5-/-* tissues exhibited no significant change in mRNA expression of *VEGFA*. Moreover, we found that *IL1A*, *IL1B*, and *IL6* expression was reduced in *ERK5-/-* tissues, which aligns with discussions on *ERK5*'s involvement in the regulation of pro-inflammatory cytokines crucial to the growth and survival of TNBC[89,90]. While we did not have time to characterize mRNA expression in 3D, and future studies from our lab will conduct this characterization in line with our methods for the cisplatin-resistant tissues, this outlines whether or not physiological relevance exists for 2D mRNA expression of *VEGFA*, as well as highlighting the need for 3D mRNA characterization, when looking at our angiogenic sprouting results.

54

While our initial experiments were confounded by the lack of locational control of spheroids in the cancer lane of our device, we found that devices with *ERK5-/-* spheroids had reduced vessel length relative to parental spheroids. Furthermore, this reduced vessel length in *ERK5-/-* devices had no statistically significant change to devices with no tumor spheroids, while parental MDA-MB-231 spheroid devices had a statistically significant increase in vessel length relative to devices with no tumor spheroids.

Taken together, the reduced vessel length from angiogenic sprouting experiments could be explained, in part, to the decreased *IL1A*, *IL1B*, and *IL6* expression in *ERK5-/-* tissues. *IL1A* and *IL1B* in particular have been shown to stimulate the expression of angiogenic factor *VEGFA* and *IL6* has been implicated in the promotion of angiogenesis in other cancer types[26,91]. Therefore, the reduction of these inflammatory genes may help explain the decrease in angiogenic sprouting due to a lack of promotion of angiogenic factors.

4.3: Future Directions

While our angiogenic sprouting assay opens a breadth of avenues for optimizing anti-angiogenic drug therapies in conjunction with cisplatin treatment, we believe further characterization and investigation is required to explore the role of additional signaling pathways implicated in drug resistance, EMT, and angiogenesis. Future research can include not only investigating different cytotoxic therapies in lung adenocarcinoma, but also for different cancer types. This could include the inclusion of more a more dynamic tumor microenvironment with additional stromal components and immune cells. Additionally with the advent of multi-organ chips, which our

55

research group is actively undertaking, the influence of other organ physiology on drug

metabolism can be modeled to see how drug resistance, EMT, and angiogenesis manifests

differentially. The inclusion of a more dynamic TME and the influence of other organs on said

TME can paint a fully characterized picture of differing factors implicated in drug resistance,

EMT, and angiogenesis. It is our hope that after such improvements are made, we can finally

translate these platforms for personalized medicine application to tailor treatment plans to the

unique genetic makeup of each patient's cancer.

APPENDIX A: PRIMER SEQUENCES

Gene	Forward Sequence (5'-->3')	Length (bp)	Tm (ºC)	Reverse Sequence	Length (bp)	Tm (ºC)
GAPDH	TTAAAAGCAGCCCTGGTGAC	20	55.5	CTCTGCTCCTCCTGTTCGAC	20	57.2
VEGFA	CGAGGGCCTGGAGTGTGT	18	59.9	CCGCATAATCTGCATGGTGAT	21	55.5
IL8	GGTGCAGTTTGCCAAGGAG	19	56.9	TTCCTTGGGGTCCAGACAGA	20	57.9
CDH1	AGGTGACAGAGCCTCTGGATAGA	23	59.4	TGGATGACACAGCGTGAGAGA	21	58.1
aSMA	CCGACCGAATGCAGAAGGA	19	57.4	ACAGAGTATTTGCGCTCCGAA	21	56.6
TGFB1	TACCTGAACCCGTGTTGCTCTC	22	58.9	GTTGCTGAGGTATCGCCAGGAA	22	59.3
EGFR1	AGGCACGAGTAACAAGCTCAC	21	57.3	ATGAGGACATAACCAGCCACC	21	57.0
PDL1	CTGGCATTTGCTGAACGCAT	20	56.9	AGGTCTTCCTCTCCATGCAC	20	56.6
IL1A	TCATTGGCGTTTGAGTCAGC	20	59.13	CCTTCATGGAGTGGGCCATA	20	59.15
IL1B	GCAGAAGTACCTGAGCTCGC	20	60.8	CTTGCTGTAGTGGTGGTCGG	20	60.67
CXCL8	AGCTCTGTGTGAAGGTGCAG	20	60.25	TTCCTTGGGGTCCAGACAGA	20	60.1
IL6	GTCCAGTTGCCTTCTCCCTG	20	60.32	CTGAGATGCCGTCGAGGATG	20	60.32
IL17A	CTGTCCCCATCCAGCAAGAG	20	60.11	AGGCCACATGGTGGACAATC	20	60.32
IL17RB	TGCACAAATACGTGGTGGTCT	21	60.2	TACAAGGAGCAGCAGCCATC	20	60.11
CXCL1	CTGGCTTAGAACAAAGGGGCT	21	60.27	TAAAGGTAGCCCTTGTTTCCCC	22	59.96
CXCL2	TTCACAGTGTGTGGTCAACATTTC	24	60.14	TCGAAACCTCTCTGCTCTAACAC	23	60.06
MMP2	TTTGAGTCCGGTGGACGATG	20	60.04	GCTCCTCAAAGACCGAGTCC	20	60.11
MMP9	GCTGCATCCAGACTTCCTCAG	21	60.74	AGGTCCTGGCAATCCCTTTGTA	22	61.37

Biography

Omar Mustafa Kamal Ahmad was born on November 19th, 1999 in Toronto, ON, Canada and raised in the Greater New Orleans area his entire life. Omar has been a research assistant in the Tissue Engineering and Microphysiological Systems (TEMPS) Lab, housed within the Department of Biomedical Engineering and Tulane Institute for Integrative Engineering for Health and Medicine (TI^{2}EHM), under the direction of Professor Mark J. Mondrinos for four years. He completed his Bachelor's of Science in Biomedical Engineering at Tulane and defended his Honor's Thesis entitled "Engineering Cisplatin Resistant Lung Adenocarcinoma Tissues" in May 2022. In April of 2022 at the American Association for Cancer Research's annual conference, Omar received third place in AACR's Undergraduate Student Poster Competition while presenting on his TEMPS Lab research, competing with over 100 students from top institutions around the country. He also received the James A. Cronvich Award and Biomedical Engineering Senior Scholar Award from Tulane's Department of Biomedical Engineering in May 2022 for his work in the TEMPS Lab. Omar is also the founder of CarBe, an automotive-technology startup allowing users to unlock their cars with their smartphone's near-field communication and biometric authentication features, and has authored two non-provisional patents related to the methods of CarBe's technology, which are actively being acquired by a global smartphone manufacturer. Omar's long term career goals are to bridge the bench-to-bedside gap in translational research, particularly with medically underserved patients, by leveraging Organ-on-a-Chip technology to start his own research group and biotech startup. Omar enjoys helping colleagues in both the TEMPS Lab and BME department, as well as traveling, photography, and new technology gadgets. Following his graduation, Omar will attend Carle Illinois School of Medicine at the University of Illinois to pursue dual MD/PhD degrees.

REFERENCES

1. Sung H, Ferlay J, Siegel RL, et al. Global Cancer Statistics 2020: GLOBOCAN Estimates of Incidence and Mortality Worldwide for 36 Cancers in 185 Countries. *CA Cancer J Clin*. 2021;71(3):209-249. doi:10.3322/caac.21660

2. Travis WD, Brambilla E, Nicholson AG, et al. The 2015 World Health Organization Classification of Lung Tumors: Impact of Genetic, Clinical and Radiologic Advances Since the 2004 Classification. *J Thorac Oncol*. 2015;10(9):1243-1260. doi:10.1097/JTO.0000000000000630

3. Molina JR, Yang P, Cassivi SD, Schild SE, Adjei AA. Non-Small Cell Lung Cancer: Epidemiology, Risk Factors, Treatment, and Survivorship. *Mayo Clin Proc*. 2008;83(5):584-594. doi:10.4065/83.5.584

4. Marra A, Viale G, Curigliano G. Recent advances in triple negative breast cancer: the immunotherapy era. *BMC Med*. 2019;17(1):90. doi:10.1186/s12916-019-1326-5

5. Dent R, Trudeau M, Pritchard KI, et al. Triple-Negative Breast Cancer: Clinical Features and Patterns of Recurrence. *Clin Cancer Res*. 2007;13(15):4429-4434. doi:10.1158/1078-0432.CCR-06-3045

6. Microfluidic organs-on-chips | Nature Biotechnology. Accessed April 28, 2023. https://www.nature.com/articles/nbt.2989

7. Esch EW, Bahinski A, Huh D. Organs-on-chips at the frontiers of drug discovery. *Nat Rev Drug Discov*. 2015;14(4):248-260. doi:10.1038/nrd4539

8. Huh D, Hamilton GA, Ingber DE. From 3D cell culture to organs-on-chips. *Trends Cell Biol*. 2011;21(12):745-754. doi:10.1016/j.tcb.2011.09.005

9. Zhang B, Radisic M. Organ-on-a-chip devices advance to market. *Lab Chip*. 2017;17(14):2395-2420. doi:10.1039/C6LC01554A

10. Ronaldson-Bouchard K, Vunjak-Novakovic G. Organs-on-a-Chip: A Fast Track for Engineered Human Tissues in Drug Development. *Cell Stem Cell*. 2018;22(3):310-324. doi:10.1016/j.stem.2018.02.011

11. Herbst RS, Morgensztern D, Boshoff C. The biology and management of non-small cell lung cancer. *Nature*. 2018;553(7689):446-454. doi:10.1038/nature25183

59

12.   Sosa Iglesias V, Giuranno L, Dubois LJ, Theys J, Vooijs M. Drug Resistance in Non-Small Cell Lung Cancer: A Potential for NOTCH Targeting? *Front Oncol*. 2018;8. Accessed April 28, 2023. https://www.frontiersin.org/articles/10.3389/fonc.2018.00267

13.   Galluzzi L, Vitale I, Michels J, et al. Systems biology of cisplatin resistance: past, present and future. *Cell Death Dis*. 2014;5(5):e1257-e1257. doi:10.1038/cddis.2013.428

14.   Sarin N, Engel F, Kalayda GV, et al. Cisplatin resistance in non-small cell lung cancer cells is associated with an abrogation of cisplatin-induced G2/M cell cycle arrest. *PloS One*. 2017;12(7):e0181081. doi:10.1371/journal.pone.0181081

15.   Pignon JP, Tribodet H, Scagliotti GV, et al. Lung Adjuvant Cisplatin Evaluation: A Pooled Analysis by the LACE Collaborative Group. *J Clin Oncol*. 2008;26(21):3552-3559. doi:10.1200/JCO.2007.13.9030

16.   Ashrafizadeh M, Zarrabi A, Hushmandi K, et al. Association of the Epithelial-Mesenchymal Transition (EMT) with Cisplatin Resistance. *Int J Mol Sci*. 2020;21(11):E4002. doi:10.3390/ijms21114002

17.   Galluzzi L, Senovilla L, Vitale I, et al. Molecular mechanisms of cisplatin resistance. *Oncogene*. 2012;31(15):1869-1883. doi:10.1038/onc.2011.384

18.   Whiteside MA, Piyathilake CJ, Bushell TM, Johanning GL. Intrinsic Cisplatin Resistance in Lung and Ovarian Cancer Cells Propagating in Medium Acutely Depleted of Folate. *Nutr Cancer*. 2006;54(2):274-284. doi:10.1207/s15327914nc5402_14

19.   Christofori G. New signals from the invasive front. *Nature*. 2006;441(7092):444-450. doi:10.1038/nature04872

20.   Dongre A, Weinberg RA. New insights into the mechanisms of epithelial–mesenchymal transition and implications for cancer. *Nat Rev Mol Cell Biol*. 2019;20(2):69-84. doi:10.1038/s41580-018-0080-4

21.   Antony J, Thiery JP, Huang RYJ. Epithelial-to-mesenchymal transition: lessons from development, insights into cancer and the potential of EMT-subtype based therapeutic intervention. *Phys Biol*. 2019;16(4):041004. doi:10.1088/1478-3975/ab157a

22.   Banyard J, Bielenberg DR. The Role of EMT and MET in Cancer Dissemination. *Connect Tissue Res*. 2015;56(5):403-413. doi:10.3109/03008207.2015.1060970

23.   Shibue T, Weinberg RA. EMT, CSCs, and drug resistance: the mechanistic link and clinical implications. *Nat Rev Clin Oncol*. 2017;14(10):611-629. doi:10.1038/nrclinonc.2017.44

24.   Hao Y, Baker D, ten Dijke P. TGF-β-Mediated Epithelial-Mesenchymal Transition and Cancer Metastasis. *Int J Mol Sci*. 2019;20(11):2767. doi:10.3390/ijms20112767

25.   Lambert AW, Weinberg RA. Linking EMT programmes to normal and neoplastic epithelial stem cells. *Nat Rev Cancer*. 2021;21(5):325-338. doi:10.1038/s41568-021-00332-6

26.   Carmeliet P, Jain RK. Molecular mechanisms and clinical applications of angiogenesis. *Nature*. 2011;473(7347):298-307. doi:10.1038/nature10144

27.   Hanahan D, Weinberg RA. Hallmarks of cancer: the next generation. *Cell*. 2011;144(5):646-674. doi:10.1016/j.cell.2011.02.013

28.   Herbst RS, Onn A, Sandler A. Angiogenesis and Lung Cancer: Prognostic and Therapeutic Implications. *J Clin Oncol*. 2005;23(14):3243-3256. doi:10.1200/JCO.2005.18.853

29.   Folkman J. Angiogenesis: an organizing principle for drug discovery? *Nat Rev Drug Discov*. 2007;6(4):273-286. doi:10.1038/nrd2115

30.   Sandler A, Gray R, Perry MC, et al. Paclitaxel–Carboplatin Alone or with Bevacizumab for Non–Small-Cell Lung Cancer. *N Engl J Med*. 2006;355(24):2542-2550. doi:10.1056/NEJMoa061884

31.   Bergers G, Hanahan D. Modes of resistance to anti-angiogenic therapy. *Nat Rev Cancer*. 2008;8(8):592-603. doi:10.1038/nrc2442

32.   McDermott M, Eustace AJ, Busschots S, et al. In vitro Development of Chemotherapy and Targeted Therapy Drug-Resistant Cancer Cell Lines: A Practical Guide with Case Studies. *Front Oncol*. 2014;4:40. doi:10.3389/fonc.2014.00040

33.   Podo F, Buydens LMC, Degani H, et al. Triple-negative breast cancer: Present challenges and new perspectives. *Mol Oncol*. 2010;4(3):209-229. doi:10.1016/j.molonc.2010.04.006

34.   Foulkes WD, Smith IE, Reis-Filho JS. Triple-Negative Breast Cancer. *N Engl J Med*. 2010;363(20):1938-1948. doi:10.1056/NEJMra1001389

35.   Isakoff SJ. Triple-Negative Breast Cancer: Role of Specific Chemotherapy Agents. *Cancer J*. 2010;16(1):53. doi:10.1097/PPO.0b013e3181d24ff7

36.   Bianchini G, Balko JM, Mayer IA, Sanders ME, Gianni L. Triple-negative breast cancer: challenges and opportunities of a heterogeneous disease. *Nat Rev Clin Oncol*. 2016;13(11):674-690. doi:10.1038/nrclinonc.2016.66

61

37.	Lehmann BD, Bauer JA, Chen X, et al. Identification of human triple-negative breast cancer subtypes and preclinical models for selection of targeted therapies. *J Clin Invest*. 2011;121(7):2750-2767. doi:10.1172/JCI45014

38.	Taube JH, Herschkowitz JI, Komurov K, et al. Core epithelial-to-mesenchymal transition interactome gene-expression signature is associated with claudin-low and metaplastic breast cancer subtypes. *Proc Natl Acad Sci*. 2010;107(35):15449-15454. doi:10.1073/pnas.1004900107

39.	Nieto MA, Huang RYJ, Jackson RA, Thiery JP. EMT: 2016. *Cell*. 2016;166(1):21-45. doi:10.1016/j.cell.2016.06.028

40.	Hoang VT, Matossian MD, Ucar DA, et al. ERK5 Is Required for Tumor Growth and Maintenance Through Regulation of the Extracellular Matrix in Triple Negative Breast Cancer. *Front Oncol*. 2020;10. Accessed January 10, 2023. https://www.frontiersin.org/articles/10.3389/fonc.2020.01164

41.	Zhang Y, Weinberg RA. Epithelial-to-mesenchymal transition in cancer: complexity and opportunities. *Front Med*. 2018;12(4):361-373. doi:10.1007/s11684-018-0656-6

42.	Chao TH, Hayashi M, Tapping RI, Kato Y, Lee JD. MEKK3 Directly Regulates MEK5 Activity as Part of the Big Mitogen-activated Protein Kinase 1 (BMK1) Signaling Pathway*. *J Biol Chem*. 1999;274(51):36035-36038. doi:10.1074/jbc.274.51.36035

43.	Finegan KG, Perez-Madrigal D, Hitchin JR, Davies C, Jordan AM, Tournier C. ERK5 is a critical mediator of inflammation-driven cancer. *Cancer Res*. 2015;75(4):742-753. doi:10.1158/0008-5472.CAN-13-3043

44.	Bhatia SN, Ingber DE. Microfluidic organs-on-chips. *Nat Biotechnol*. 2014;32(8):760-772. doi:10.1038/nbt.2989

45.	GRAYSON ACR, SHAWGO RS, JOHNSON AM, et al. A BioMEMS review: MEMS technology for physiologically integrated devices. *Proc IEEE*. 2004;92(1):6-21. doi:10.1109/JPROC.2003.820534

46.	Whitesides GM. The origins and the future of microfluidics. *Nature*. 2006;442(7101):368-373. doi:10.1038/nature05058

47.	Jang KJ, Suh KY. A multi-layer microfluidic device for efficient culture and analysis of renal tubular cells. *Lab Chip*. 2010;10(1):36-42. doi:10.1039/B907515A

62

48.   Huh D, Matthews BD, Mammoto A, Montoya-Zavala M, Hsin HY, Ingber DE. Reconstituting Organ-Level Lung Functions on a Chip. *Science*. 2010;328(5986):1662-1668. doi:10.1126/science.1188302

49.   Ingber DE. Reverse Engineering Human Pathophysiology with Organs-on-Chips. *Cell*. 2016;164(6):1105-1109. doi:10.1016/j.cell.2016.02.049

50.   Zhao Y, Rafatian N, Wang EY, et al. Towards chamber specific heart-on-a-chip for drug testing applications. *Adv Drug Deliv Rev*. 2020;165-166:60-76. doi:10.1016/j.addr.2019.12.002

51.   Ronaldson-Bouchard K, Teles D, Yeager K, et al. A multi-organ chip with matured tissue niches linked by vascular flow. *Nat Biomed Eng*. 2022;6(4):351-371. doi:10.1038/s41551-022-00882-6

52.   Hassan S, Sebastian S, Maharjan S, et al. Liver-on-a-Chip Models of Fatty Liver Disease. *Hepatology*. 2020;71(2):733. doi:10.1002/hep.31106

53.   Low LA, Tagle DA. Organs-on-chips: Progress, challenges, and future directions. *Exp Biol Med*. 2017;242(16):1573-1578. doi:10.1177/1535370217700523

54.   Zhang B, Korolj A, Lai BFL, Radisic M. Advances in organ-on-a-chip engineering. *Nat Rev Mater*. 2018;3(8):257-278. doi:10.1038/s41578-018-0034-7

55.   Jang KJ, Otieno MA, Ronxhi J, et al. Reproducing human and cross-species drug toxicities using a Liver-Chip. *Sci Transl Med*. 2019;11(517):eaax5516. doi:10.1126/scitranslmed.aax5516

56.   Sung JH, Wang Y, Shuler ML. Strategies for using mathematical modeling approaches to design and interpret multi-organ microphysiological systems (MPS). *APL Bioeng*. 2019;3(2):021501. doi:10.1063/1.5097675

57.   Homan KA, Kolesky DB, Skylar-Scott MA, et al. Bioprinting of 3D Convoluted Renal Proximal Tubules on Perfusable Chips. *Sci Rep*. 2016;6(1):34845. doi:10.1038/srep34845

58.   Zhang YS, Arneri A, Bersini S, et al. Bioprinting 3D microfibrous scaffolds for engineering endothelialized myocardium and heart-on-a-chip. *Biomaterials*. 2016;110:45-59. doi:10.1016/j.biomaterials.2016.09.003

59.   Bhise NS, Ribas J, Manoharan V, et al. Organ-on-a-chip platforms for studying drug delivery systems. *J Controlled Release*. 2014;190:82-93. doi:10.1016/j.jconrel.2014.05.004

63

60.   Derakhshanfar S, Mbeleck R, Xu K, Zhang X, Zhong W, Xing M. 3D bioprinting for biomedical devices and tissue engineering: A review of recent trends and advances. *Bioact Mater*. 2018;3(2):144-156. doi:10.1016/j.bioactmat.2017.11.008

61.   Knowlton S, Onal S, Yu CH, Zhao JJ, Tasoglu S. Bioprinting for cancer research. *Trends Biotechnol*. 2015;33(9):504-513. doi:10.1016/j.tibtech.2015.06.007

62.   Xia Y, Whitesides GM. Soft Lithography. *Angew Chem Int Ed*. 1998;37(5):550-575. doi:10.1002/(SICI)1521-3773(19980316)37:5<550::AID-ANIE550>3.0.CO;2-G

63.   Qin D, Xia Y, Whitesides GM. Soft lithography for micro- and nanoscale patterning. *Nat Protoc*. 2010;5(3):491-502. doi:10.1038/nprot.2009.234

64.   Kim S, Lee H, Chung M, Jeon NL. Engineering of functional, perfusable 3D microvascular networks on a chip. *Lab Chip*. 2013;13(8):1489-1500. doi:10.1039/C3LC41320A

65.   Vlachogiannis G, Hedayat S, Vatsiou A, et al. Patient-derived organoids model treatment response of metastatic gastrointestinal cancers. *Science*. 2018;359(6378):920-926. doi:10.1126/science.aao2774

66.   Sontheimer-Phelps A, Hassell BA, Ingber DE. Modelling cancer in microfluidic human organs-on-chips. *Nat Rev Cancer*. 2019;19(2):65-81. doi:10.1038/s41568-018-0104-6

67.   Hassell BA, Goyal G, Lee E, et al. Human Organ Chip Models Recapitulate Orthotopic Lung Cancer Growth, Therapeutic Responses, and Tumor Dormancy In Vitro. *Cell Rep*. 2017;21(2):508-516. doi:10.1016/j.celrep.2017.09.043

68.   Pavesi A, Tan AT, Koh S, et al. A 3D microfluidic model for preclinical evaluation of TCR-engineered T cells against solid tumors. *JCI Insight*. 2017;2(12). doi:10.1172/jci.insight.89762

69.   Sackmann EK, Fulton AL, Beebe DJ. The present and future role of microfluidics in biomedical research. *Nature*. 2014;507(7491):181-189. doi:10.1038/nature13118

70.   Prantil-Baun R, Novak R, Das D, Somayaji MR, Przekwas A, Ingber DE. Physiologically Based Pharmacokinetic and Pharmacodynamic Analysis Enabled by Microfluidically Linked Organs-on-Chips. *Annu Rev Pharmacol Toxicol*. 2018;58(1):37-64. doi:10.1146/annurev-pharmtox-010716-104748

71.   Cooper JA. Effects of cytochalasin and phalloidin on actin. *J Cell Biol*. 1987;105(4):1473-1478. doi:10.1083/jcb.105.4.1473

72.   Scholzen T, Gerdes J. The Ki-67 protein: From the known and the unknown. *J Cell Physiol*. 2000;182(3):311-322. doi:10.1002/(SICI)1097-4652(200003)182:3<311::AID-JCP1>3.0.CO;2-9

73.   Neurohr GE, Terry RL, Lengefeld J, et al. Excessive Cell Growth Causes Cytoplasm Dilution And Contributes to Senescence. *Cell*. 2019;176(5):1083-1097.e18. doi:10.1016/j.cell.2019.01.018

74.   David JM, Dominguez C, Hamilton DH, Palena C. The IL-8/IL-8R Axis: A Double Agent in Tumor Immune Resistance. *Vaccines*. 2016;4(3):22. doi:10.3390/vaccines4030022

75.   Sato M, Larsen JE, Lee W, et al. Human Lung Epithelial Cells Progressed to Malignancy through Specific Oncogenic Manipulations. *Mol Cancer Res*. 2013;11(6):638-650. doi:10.1158/1541-7786.MCR-12-0634-T

76.   Du B, Shim JS. Targeting Epithelial–Mesenchymal Transition (EMT) to Overcome Drug Resistance in Cancer. *Molecules*. 2016;21(7):965. doi:10.3390/molecules21070965

77.   Wang J, Wang B, Chu H, Yao Y. Intrinsic resistance to EGFR tyrosine kinase inhibitors in advanced non-small-cell lung cancer with activating EGFR mutations. *OncoTargets Ther*. 2016;9:3711-3726. doi:10.2147/OTT.S106399

78.   Zhang P, Ma Y, Lv C, et al. Upregulation of programmed cell death ligand 1 promotes resistance response in non-small-cell lung cancer patients treated with neo-adjuvant chemotherapy. *Cancer Sci*. 2016;107(11):1563-1571. doi:10.1111/cas.13072

79.   Merchant N, Nagaraju GP, Rajitha B, et al. Matrix metalloproteinases: their functional role in lung cancer. *Carcinogenesis*. 2017;38(8):766-780. doi:10.1093/carcin/bgx063

80.   Barr MP, Gray SG, Hoffmann AC, et al. Generation and characterisation of cisplatin-resistant non-small cell lung cancer cell lines displaying a stem-like signature. *PloS One*. 2013;8(1):e54193. doi:10.1371/journal.pone.0054193

81.   Wangpaichitr M, Wu C, You M, et al. Inhibition of mTOR restores cisplatin sensitivity through down-regulation of growth and anti-apoptotic proteins. *Eur J Pharmacol*. 2008;591(1):124-127. doi:10.1016/j.ejphar.2008.06.028

82.   Witta SE, Gemmill RM, Hirsch FR, et al. Restoring E-Cadherin Expression Increases Sensitivity to Epidermal Growth Factor Receptor Inhibitors in Lung Cancer Cell Lines. *Cancer Res*. 2006;66(2):944-950. doi:10.1158/0008-5472.CAN-05-1988

65

83.   Wang J, Chen Y, Xiang F, et al. Suppression of TGF-β1 enhances chemosensitivity of cisplatin-resistant lung cancer cells through the inhibition of drug-resistant proteins. *Artif Cells Nanomedicine Biotechnol*. 2018;46(7):1505-1512. doi:10.1080/21691401.2017.1374285

84.   Zhou P, Hu J, Wang X, Wang J, Zhang Y, Wang C. Epidermal growth factor receptor expression affects proliferation and apoptosis in non-small cell lung cancer cells via the extracellular signal-regulated kinase/microRNA 200a signaling pathway. *Oncol Lett*. 2018;15(4):5201-5207. doi:10.3892/ol.2018.7961

85.   Xu G, Yu H, Shi X, et al. Cisplatin sensitivity is enhanced in non-small cell lung cancer cells by regulating epithelial-mesenchymal transition through inhibition of eukaryotic translation initiation factor 5A2. *BMC Pulm Med*. 2014;14(1):174. doi:10.1186/1471-2466-14-174

86.   Langhans SA. Three-Dimensional in Vitro Cell Culture Models in Drug Discovery and Drug Repositioning. *Front Pharmacol*. 2018;9. Accessed May 4, 2023. https://www.frontiersin.org/articles/10.3389/fphar.2018.00006

87.   Folkman J. Tumor Angiogenesis: Therapeutic Implications. *N Engl J Med*. 1971;285(21):1182-1186. doi:10.1056/NEJM197111182852108

88.   Yang W, Bai J, Liu D, et al. MiR-93-5p up-regulation is involved in non-small cell lung cancer cells proliferation and migration and poor prognosis. *Gene*. 2018;647:13-20. doi:10.1016/j.gene.2018.01.024

89.   Esquivel-Velázquez M, Ostoa-Saloma P, Palacios-Arreola MI, Nava-Castro KE, Castro JI, Morales-Montor J. The Role of Cytokines in Breast Cancer Development and Progression. *J Interferon Cytokine Res*. 2015;35(1):1-16. doi:10.1089/jir.2014.0026

90.   Rovida E, Maira GD, Tusa I, et al. The mitogen-activated protein kinase ERK5 regulates the development and growth of hepatocellular carcinoma. *Gut*. 2015;64(9):1454-1465. doi:10.1136/gutjnl-2014-306761

91.   DeRose YS, Gligorich KM, Wang G, et al. Patient-derived models of human breast cancer: protocols for in vitro and in vivo applications in tumor biology and translational medicine. *Curr Protoc Pharmacol*. 2013;Chapter 14:Unit14.23. doi:10.1002/0471141755.ph1423s60